Instituto Nacional de Astrofísica, Optica y Electrónica.

"Acoustic Rotational Streaming and Angular Momentum Transfer to Matter driven by Ultrasonic Acoustic Vortices"

By

Lic. Juan Israel Vázquez Lozano

Thesis submitted as requirements to obtain the degree of

MASTER IN OPTICS

Thesis advisor:

Dr Rubén Ramos García
INAOE

Sta. María Tonantzintla, Puebla, México
August, 2015

A mis padres, gracias por siempre estar ahí.

Learn from yesterday, live for today, hope for tomorrow.

The important thing is not to stop questioning.

– Albert Einstein

Acknowledgements

First of all, I would like to thank God for all the opportunities that He has given me during my life.

Thanks to my mother Mrs. Guadalupe Lozano Pérez for showing me what strength is, for motivating me to keep on forward no matter how hard it seems. For its infinite love and comprehension. For her unconditional support. There is no better example of life for me.

To my father Dr. Juan José Vázquez Tovar for supporting every an each one of my decisions. For pushing me up until the end and teaching me to fight untiringly to reach my goals and accomplish my dreams. Thank you for teaching me until the very last moment that the most humble man can leave unforgettable teachings to hundreds of peoples.

To my Thesis advisors, Dr. Rubén Ramos Garcia for his support and thrust. Thanks for letting me live this amazing experience full of personal and intellectual growth. Thanks to Prof. Régis Wunenburger for his hospitality, for giving me the necessary tools, the thrust and support during all my internship in Paris. Also thanks to Dr. Etienne Brasselet for all his advises and thrust along the evolution of the work.

To my brothers Edgar and Ivan because no matter how far we are, their love and care is always present.

To my grandparents, Dr. Jorge Vázquez, Ma. Luisa Tovar, Jesús Lozano and Margarita Pérez for their example and teachings during all my life.

To all my family and friends old and new, for all the love and support through the most difficult times of my life, for being there to help me and lift me when necessary.

Thanks to all the people from INAOE and UPMC, co-workers and administrative people whom effort made my internship possible, thank you very much.

Agradecimientos

En primer lugar agradecer a Dios por todas las oportunidades que me ha brindado a lo largo de mi vida.

A mi madre Mtra. Maria Guadalupe Lozano Pérez, por demostrarme lo que es la fortaleza, por motivarme a seguir adelante sin importar que tan duro se vea el camino. Por su infinito amor y comprensión. Por su apoyo incondicional. No existe un mejor ejemplo para mí.

A mi padre, Dr. Juan José Vázquez Tovar, por apoyar todas y cada una de mis decisiones. Por apoyarme hasta el final y enseñarme a luchar incansablemente para alcanzar nuestras metas y cumplir nuestros sueños. Por enseñarme hasta el último momento que el hombre más humilde puede dejar una marca imborrable en cientos de personas.

A mis asesores, el Dr. Rubén Ramos García por su apoyo y su confianza. Por permitirme vivir una experiencia increíble llena de crecimiento intelectual y personal. Al Prof. Régis Wunenburger por su hospitalidad, por brindarme las herramientas necesarias, la confianza y el apoyo a lo largo de mi estancia de investigación. Al Dr. Etienne Brasselet, por sus consejos y confianza a lo largo del desarrollo de este trabajo.

A mis hermanos, que no importa cuán lejos estén su amor y cariño siempre está presente.

A mis abuelitos, Dr. Jorge Vázquez, Ma. Luisa Tovar, Jesús Lozano y Margarita Pérez por sus ejemplos y enseñanzas a lo largo de mi vida, siempre estaré agradecido.

A mis familiares y amigos de la familia por todo su apoyo y buenos deseos.

A mis amigos, lo viejos conocidos y los nuevos, por tanto apoyo y cariño A los de toda la vida: Mau, Chava, Peri, Arturo, Jose, Marco, Julián. A la chaviza: Noé, Justine, Pollo, Roy, Carrits, por su amistad. A los Yolos de Tonantzintla, por emprender este viaje juntos, por su amistad y cariño- A los Mexas de París, amigos que en poco tiempo se volvieron hermanos lejos de nuestro ambiente natural. A Sandra, Nax, Gaby, Fer, Sergio, Andrea, Normita, Polo, Alejandro, Iván y todos aquellos que me brindaron su cariño y apoyo en los momentos más difíciles de mi vida. A todos y cada uno les estoy eternamente agradecido.

A todas las personas en INAOE y en UPMC, compañeros, administrativos y todos aquellos que hicieron posible mi estancia, muchas gracias.

Abstract

Mechanical effects of waves on material media is a powerful option to achieve contactless manipulation in a controlled manner, which has already found numerous applications in optics and acoustics. A basic example consists of absorption-mediated wave-matter exchange of linear and/or angular momentum that light or sound may carry. To date, the demonstration of all kinds of exchanges mediated by dissipative processes have been carried out experimentally. Moreover, non-dissipative exchanges of linear and angular momentum between waves and matter are also possible.

Furthermore, recent works have observed indirectly that acoustic vortices impart momentum to a fluid unveiling a rotational flow of the liquid. This rotational flow is the counterpart of the classical acoustic streaming, which is the linear motion along the beam propagation direction that results from momentum transfer due to thermoviscous dissipations induced sound absorption. This rotational flow induced by the radiation torque exerted on the sound absorbing fluid through which the acoustic beam propagates, circulates around the propagation direction of the acoustic vortex.

First we report on orbital angular momentum exchange between sound and matter mediated by a non-dissipative chiral scattering process. The experimental demonstration is made by irradiating a three-dimensional printed, spiral-shaped chiral object using an incident ultrasonic beam carrying zero orbital angular momentum. This is the acoustic analog of an optical spiral phase plate (SPP) but for sound waves. Chiral refraction is shown to impart a nonzero orbital angular momentum to the scattered field and to rotate the object. This result constitutes a proof-of-concept of a novel kind of acoustic angular manipulation of matter.

After that, we report the first direct experimental demonstration of acoustic rotational streaming as result of the exchange of momentum between an acoustic vortex and fluid with PMMA particles used as tracers of the flow. It is shown that the system behaves as a Fabry –Pérot like cavity for acoustic waves. Experimental results and observations are sustained by a small model developed for the system providing a first approach to this phenomenon.

Index

Chapter 1

Introduction

Electromagnetic radiation and sound are fundamental entities of our world. They are related to almost any phenomena that we can imagine. Almost any interaction or exchange involves at least one of these two elements. Moreover, they both have analogous properties in which mankind has based the development of its recent technology.

It is well known that, both light and sound, carry linear and angular momentum and that this momentum can be used in many circumstances, in which the transfer of momentum to matter has a variety of applications in diverse fields.

On the one hand, the transfer of the linear momentum of waves to matter results in a radiation force that enables to control the position of objects and possibly deform them. On the other hand, the transfer of angular momentum results in a radiation torque that can be used to rotate material systems.

Mechanical effects of waves on material media is a powerful option to achieve contactless manipulation in a controlled manner, which has already found numerous applications in optics and acoustics. A basic example consists of absorption-mediated wave-matter exchange of linear and/or angular momentum that light or sound may carry, from which radiation force and/or torque take place. To date, the demonstration of all kinds of exchanges mediated by dissipative processes have been carried out experimentally.

That light carries momentum is known from the work of Maxwell and later of Planck and Einstein. Since the 1970s light's linear moment has been used in optical manipulation experiments. Light has also been shown to carry angular momentum: spin angular momentum related to the polarization state of the light and, more recently, orbital angular momentum, as a result of helicity in the phase fronts of the light. Sound, being a longitudinal wave, carries no spin component but can carry an orbital component of angular momentum when endowed with an appropriate phase structure.

In recent years, the study of waves which carry angular momentum has gained interest in the scientific community, its generation and applications in several areas of knowledge give a huge motivation to search and find more properties suitable in the development of science.

As its analog in electromagnetism, acoustic Orbital Angular Momentum (OAM) is an unique property of acoustic waves. The OAM carried by an acoustic wave can be varied only by exchange with the medium through which it propagates, either by absorption or space-variant properties of the medium. The OAM transfer from an acoustic wave to matter results in a torque, which is called the "radiation torque" by analogy with the radiation pressure associated with the transfer of linear momentum of a wave. Generally speaking, since the radiation torque exerted on matter by an electromagnetic or acoustic wave is proportional to P/ω, where P is the beam power and ω its angular frequency, it is anticipated that acoustic radiation torques are 10^9 larger than optical radiation torques for a given P. Similarly, in the case of OAM transfer by absorption, the associated heating is proportional to ω. Thus, the heating induced by OAM transfer through absorption is expected to be 10^9 smaller for acoustics than for optics for a given absorption. Finally, the usual ultrasonic wavelengths are within the millimeter range. For these reasons, a large application potential of acoustic OAM to the manipulation of matter at the macroscopic scale is anticipated, e.g. contactless acoustics driven pumps and valves, micromixing, trapping, etc.

Several groups have already theoretically investigated the properties of acoustic beams carrying OAM. A representative class of such beams corresponds to acoustic fields endowed with a phase singularity, commonly called "acoustic vortices" [figure 1]. However, much less has been done experimentally. Still, one can mention a few demonstrations of the generation of acoustic vortices using acousto-optic interaction [1, 2], spiral-shaped mono-element transducers [3], multi-element transducers [3, 4]. More recently, researchers have started to use the OAM carried by acoustic vortices to impart a solid rotation to freely rotating solid objects thanks to the radiation torque exerted by the acoustic vortices on the solids. This has first been demonstrated in the kHz frequency range for sound absorbing

solids surrounded by air in 2008 [5, 6] and very recently extended to MHz frequency range for sound absorbing solids immersed in fluids in 2012 [7, 8]. Intriguingly, the demonstration of an exchange of angular momentum between sound and matter that is not mediated by absorption has not yet been reported. Here we aim at filling this gap by observing experimentally the direct signature of the phenomenon both for the material medium and the acoustic field.

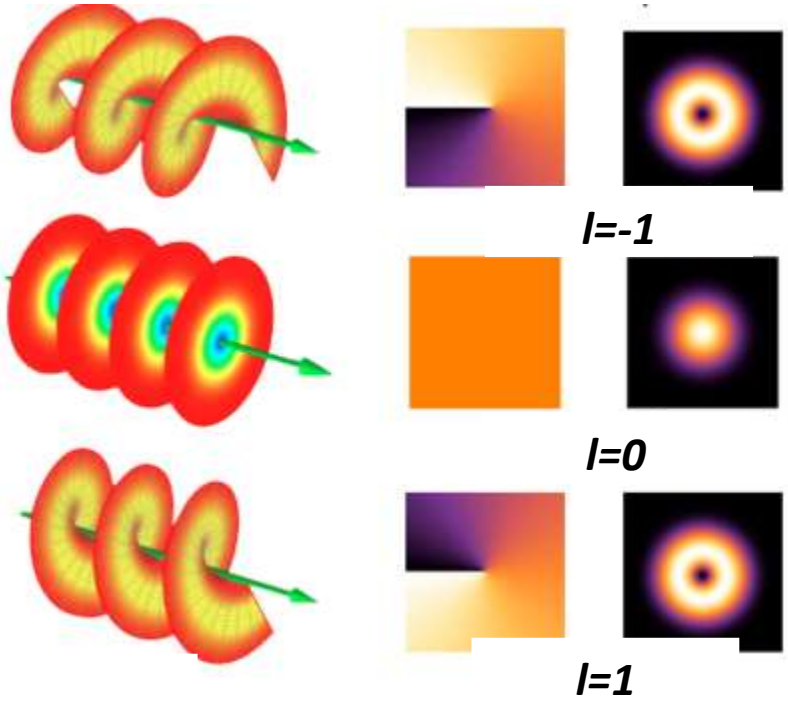

Figure 1. Helical wave, its intensity pattern and phase for topological charges $l = -1,0,1$.

The principle of our demonstration relies on the use of a chiral object having the form of a spiral phase plate (SPP). This is the acoustic analog of an optical SPP [10].

Intriguingly, recent experimental investigations [8] have indirectly unveiled a rotational flow of the liquid in which is immersed the solid put into rotation by acoustic OAM. This rotational flow is the counterpart of the classical “acoustic streaming”, which is the linear fluid motion along the beam propagation direction that results from linear momentum transfer from sound to the fluid due to thermoviscous dissipation induced sound absorption [9]. This rotational flow induced by the radiation torque exerted on the sound absorbing fluid through which the acoustic beam propagates, circulates around the propagation direction of the acoustic vortex.

Quite naturally, this effect has been referred to as “acoustic rotational streaming” and remains to be explored quantitatively. The main goal of the project is to achieve the first direct experimental demonstration and quantitative study of acoustic rotational streaming in a viscous fluid.

1.2 Motivation

Explore and fill the gaps in the study of acoustic vortices and its interaction with matter and liquids. This means generation of acoustic vortices through the interaction between an acoustic plane wave and an object with and specific shape designed by the user.

Unveil the phenomenon known as rotational acoustic streaming to use it as a new technique for manipulation of matter and diverse applications.

Achieve the first direct experimental demonstration and quantitative study of acoustic rotational streaming in a viscous fluid, its properties and a basic theory for its understanding.

1.3 Objectives

- Observe and identify the exchange of angular momentum between an acoustic wave and matter by chiral scattering
- Identify the correct parameters to fulfill the observation of an acoustic vortex and rotation of matter due to this exchange of momentum
- Build a set up to generate and observe acoustic rotational streaming
- If possible, characterize the system and build a mathematical model of the observed behaviors

In the present work an experimental demonstration of the interaction between an acoustic plane wave and a polymer disk with a specific shape give rise to an acoustic vortex and transfer of momentum to the disk. This providing the first demonstration of an exchange of angular momentum between sound and matter that is not mediated by absorption.

The second part of the work is oriented to show the first direct observation of rotational acoustic streaming and the characterization of the system.

In general, the content of this thesis is organized as follows. First, in chapter 2, an overview of the theory involving wave vortices will be established. Solutions of the wave equation and an explanation on the exchange of momentum between matter and sound will be given. In this chapter a brief explanation on streaming and flow will be described.

The experimental set up and characteristics of both systems used during the project will be shown and explained in chapter 3. A brief description of the elements used and the characterization of the transducer will be shown.

Results obtained of all the experimental experience, their diskussion and possible mathematical explanation are presented in chapter 4.

Finally, the conclusions, a general outlook and recommended future work on the thesis will be presented in chapter 5.

1.4 References

[1] S. Gspan, A. Meyer, S. Bernet, M. Ritsch-Marte, Optoacoustic generation of a helicoidal ultrasonic beam. J. Ac. Soc. Am. 115, 1142 (2004)

[2] P. Z. Datshi, F. Alhassen, H. P. Lee, Observation of orbital angular momentum transfer between acoustic and optical vortices in optical fiber, Phys. Rev. Lett. 96, 043604

[3] B. T. Hefrner, P. L. Marston, An acoustical helicoidal wave transducer with applications for the alignment of ultrasonic and underwater systems. J. Ac. Soc. Am. 106, 3313 (1999).

[4] R. Marchiano, J. L. Thomas, Synthesis and analisys of linear and nonlinear acoustical vortices, Phys. Rev. E 71, 066616 (2005).

[5] K. Volke-Sepulveda, A. O. Santillan, R. R. Boullosa, Transfer of angular momentum to matter from acoustical vortices in free space, Phys. Rev. Lett. 100, 024302 (2008).

[6] K. D. Skeldon, C. Wilson, M. Edgar, M. J. Padgett, An acoustical spanner and its associated rotational Doppler shift, New J. Phys. 10, 013018 (2008).

[7] C. E. M. Delmore, Z. Yang, A. Volovick, S. Cochran, M. P. MacDonald, G. C. Spalding, Mechanical evidence of the orbital angular momentum to energy ratio of vortex beams, Phys. Rev. Lett. 108, 194301 (2012).

[8] A. Anhaueser, R. Wunenburger, E. Brasselet, Acoustic rotational manipulation using orbital angular momentum transfer, Phys. Rev Lett. 109, 034301 (2012).

[9] M. F. Hamilton, D. T. Blackstock, Nonlinear Acoustics, Academic Press, (1998).

[10] M. W. Beijersbergen, R. P. C. Coerwinkel, M. Kristensen, J. P. Woerdman, Helical-wavefront laser beams produced with a spiral phaseplate, Opt. Commun. 112, 321 (1994).

Chapter 2

State of Art

In this chapter, the basic theory that sustains the project is presented. The solution of the sound wave equation is presented as the generalized Bessel beams. After that, the explanation of the exchange of momentum is presented and its proportionality with the topological charge of a beam.

To understand the phenomenon behind the generation of the acoustic vortex from the exchange of angular momentum between the acoustic wave and the object used, it is necessary to review two fundamental concepts involved: conservation and exchange of angular momentum and torque.

2.1 Acoustic vortices and edge dislocations

Phase singularities can be classified into three types: Edge dislocations, screw dislocations and the general type, mixed edge-screw dislocations [2]. Their name refers to structural similarities with crystal defects. A screw dislocation, also refered as helicoidal wave or vortex, is an axis parallel to the propagation direction around which the wave has a phase dependence $e^{il\theta}$ of the polar angle θ where l is an integer [3] and it is called the topological charge of the vortex. The wavefronts are $|l|$ helices winding around the axis with a slope of l, the sign of l determining their handedness. The wavefronts of vortices of charges 1, 2 and 3 are shown in figure 1. On a closed (counterclockwise) circuit about the beam axis, the phase rises $2\pi l$. On the axis itself, the phase is undetermined and the amplitude is zero [2]. At that point, the amplitude of the wave field is null and it forms a dark core because of destructive interference.

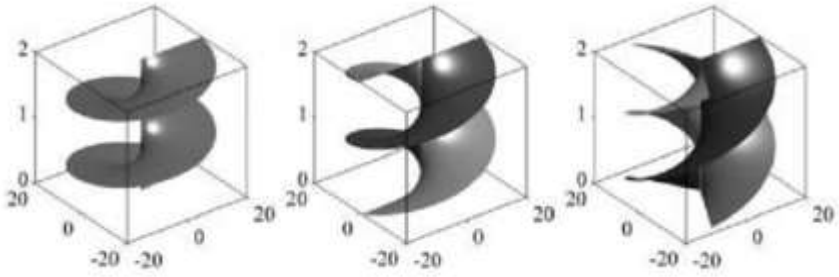

Figure 1. Wavefronts for a AVs of topological charge 1, 2 and 3, respectively. The vertical unit is λ, the others are arbitrary. [1]

2.2 Sound wave equation. Generalized Bessel beams

When it comes to sound waves, several describing models can be used in order to approximate reality with theoretical calculus.

From now on to describe sound waves considered in the experiment, simplified description of beams will be used. Generalized Bessel beams model will be applied to represent the acoustic pressure field p, this as a consequence of using a spherical transducer in which the use of cylindrical coordinates is appropriate.

It is well known that linear sound is represented by solutions of the homogeneous wave equation:

$$\nabla^2\psi - d_{ct}^2\psi = 0 \tag{2.1}$$

where ψ is a complex velocity potential. In a fluid, the first-order fluid velocity is given by the gradient of either the real or imaginary part of ψ [6]. Consider single frequency solutions of (2.1) expressed in cylindrical polar coordinates (r,z,θ), where $r = \sqrt{x^2 + y^2}$ is the distance from the z axis:

$$\psi(r,t) = e^{-i\omega t}\psi(r) \tag{2.2}$$

$\psi(r)$ is chosen to be harmonic and to satisfy the Helmholtz equation

$$\nabla^2\psi - K^2\psi = 0 \tag{2.3}$$

$$K = \frac{\omega}{c}$$

The generalized Bessel beam is a family of exact solutions of (2.1) of the form:

$$\psi(r,t) = e^{-i\omega t}\psi_n(r) \tag{2.4}$$

With

$$\psi_n(r) = e^{in\theta}\int_0^K f(k)e^{iqz}J_n(kr)dk \tag{2.5}$$

$$K^2 = k^2 + q^2$$

Thereby, expression (2.4) can be written as:

$$\psi_n(r,t) = e^{i(qz-\omega t)}e^{in\theta}\int_0^K f(k)J_n(kr)dk \tag{2.6}$$

For the purpose of the thesis, there is no intention to stress the amplitude contribution (of none exponential forms $f(k)$) to $\psi(r,t)$ given that the range of k ensures that both k and q are real [6], so there are no terms with exponentially increasing or decreasing amplitude. Expression (2.6) will be expressed as:

$$\psi(r,t) = e^{i(qz-\omega t)}e^{il\theta}A(r) \tag{2.7}$$

Being $A(r) = re^{-r^2}$ the amplitude without exponential influence within a paraxial aproximation, as has been mentioned above. Solutions of (2.1) of the form (2.7) are considered to represent lineal sound propagation of the system. The profile and phase of a vortex wave with a topological charge equal to $l = 1$ is shown in figure 2.

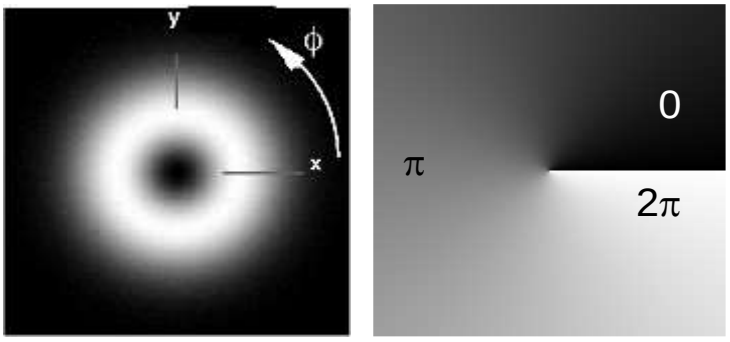

Figure 2. Amplitude and phase of a vortex with a topological charge $l = 1$

2.3 Proportionality between the angular momentum and the topological charge of a beam with azimuthal dependence

Generalized Bessel beams have been used to demonstrate the proportionality between the angular momentum carried by an acoustic vortex (AV) and its topological charge l [5]. Knowing that momentum density is

$$\vec{L} = (\vec{r} \times \rho\vec{v}) \tag{2.8}$$

Where $\rho\vec{v}$ is the linear momentum p_m.

Recalling the theory concerning acoustic waves in fluids [5], the energy density of the wave under certain conditions for a helical wave like (2.4) can be expressed as

$$\overline{e}(r) = \frac{1}{4}\rho_0[|\nabla\psi|^2 + K^2|\psi|^2] \tag{2.9}$$

This equation satisfies that its momentum density averaged in time can be expressed in the form

$$\overrightarrow{p(r)} = \rho\overline{\mathrm{v}} = \frac{\kappa\rho}{2c} Im(\psi^*\nabla\psi) \tag{2.10}$$

Assuming z as the propagation axis of the acoustic vortex (AV) beam, the cycle-averaged angular momentum is:

$$\vec{L}_z = (\vec{r} \times \vec{p}_m\,)_z = xp_y - yp_x = rp_\theta \tag{2.11}$$

Noting that L_z is zero unless ψ has azimuthal dependence therefore

$$\overrightarrow{L_z} = \frac{\kappa\rho}{2c} Im(\psi^*\partial_\theta\psi) \tag{2.12}$$

In Generalized Bessel beams, the azimuthal dependence is entirely in the factor $e^{il\theta}$ then (2.12) becomes

$$\vec{L}_z = \frac{\kappa\rho}{2c} l|\psi|^2 \tag{2.13}$$

In which case is demonstrated that the cycle-averaged angular momentum density of the AV beam is proportional to the topological charge l.

2.4 Momentum. Conservation and exchange

Angular momentum can be expressed as its linear momentum, mv, cross multiplied by its position from the origin, r. [7] Thus, the angular momentum (OAM) L of a particle with respect to some point of origin is

$$\vec{L} = (\vec{r} \times m\vec{v}) \tag{2.14}$$

It can also be expressed as the product of the body's moment of inertia, I_z and its angular velocity Ω_z:

$$\vec{L} = I_z\overrightarrow{\Omega_z} \tag{2.15}$$

The experiment developed is considered as an isolated and closed system where no external torques or forces act on it. Hence, the conservation of angular momentum, implied by Newton's law, states that total angular momentum is conserved. [8]

The angular momentum of the system before and event ($\vec{L}_A$) involving only internal torques is equal to the angular momentum of the system after the event ($\vec{L}_B$).

$$\sum \vec{L}_A = \sum \vec{L}_B \tag{2.16}$$

Considering the existence of the system with two particles named particle 1 and particle 2:

$$\sum \vec{L}_A = \vec{L}_{A1} + \vec{L}_{A2} \tag{2.17}$$

Following second Newton's law [9], principle of action reaction:

$$\vec{L}_{A1} = -\vec{L}_{A2}$$

$$\vec{L}_{A1} + \vec{L}_{A2} = 0$$

$$\sum \vec{L}_A = \vec{L}_{A1} + \vec{L}_{A2} = 0 \tag{2.18}$$

$$\sum \vec{L}_A = \sum \vec{L}_B = 0; \qquad \vec{L}_{system} = constant \tag{2.19}$$

2.5 Torque

The time derivative of angular momentum is called torque Γ. It is defined as the cross product of the value of the distance from rotation axis r and the force F received perpendicularly to distance r. [10]

$$\vec{\Gamma} = \frac{d\vec{L}}{dt} = \vec{r} \times \vec{F} \tag{2.20}$$

If $L_{system} = constant$, then

$$\sum \vec{\Gamma}_{external} = 0 \tag{2.21}$$

$$\frac{d\vec{L}_{system}}{dt} = \sum \vec{\Gamma}_{external} \tag{2.22}$$

2.6 Generation of an acoustic vortex: Exchange of angular momentum between a spiral phase plate and an acoustic plane wave.

Phase modulation of an acoustic wave allows one to obtain an acoustic vortex. The element considered to introduce this phase modulation is a spiral plate, an analogous of a phase plate in optics. Considering the system formed by the spiral and an acoustic

wave as an isolated and closed system, the exchange of momentum can be demonstrated [14]. The diagram of the system is shown in figure 3.

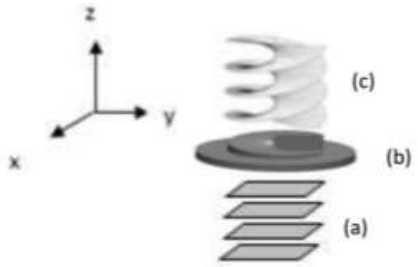

Figure 3. (a) Plane isophase surfaces of an acoustic regular beam emitted by a transducer which direction of propagation is the Z axis. Without azimuthal dependence. (b) Polymer material with spiral shape. Its -θ variant design will cause a phase delay to the wave that trespasses it. (c) Resulting beam after crossing the spiral has become an Acoustic vortex, characterized by its azimuthal dependent amplitude factor $e^{in\theta}$.

The angular momentum (in the z direction) of the system before the wave crosses the spiral ($\vec{L}_{z\_beforeSpiral}$) involving only internal torques, is equal to the angular momentum of the system after crossing the spiral ($\vec{L}_{z\_afterSpiral}$).

$$\sum \vec{L}_{z_{beforeSpiral}} = \sum \vec{L}_{z_{afterSpiral}} \tag{2.23}$$

This process can be divided into two moments, the wave before the spiral and after the spiral.

Before the wave passes through the spiral one has

$$\sum \vec{L}_{z_{beforeSpiral}} = \vec{L}_{z_{Spiral}} + \vec{L}_{z_{Beam}} \tag{2.24}$$

As no external forces are considered

$$\vec{L}_{z_{Spiral}} = 0$$

Regarding the angular momentum of the upstream beam, no azimuthal dependence exists. Hence no angular momentum.

$$\vec{L}_{z_{Beam}} = 0$$

Being

$$\sum \vec{L}_{z_{beforeSpiral}} = \vec{L}_{z_{Spiral}} + \vec{L}_{z_{Beam}} = 0 \tag{2.25}$$

After the spiral the situation changes as follows:

$$\sum \vec{L}_{z_{afterSpiral}} = \vec{L}_{z_{Spiral}} + \vec{L}_{z_{Beam}}$$

In that case, the beam downstream the spiral has azimuthal dependence carrying angular momentum as shown in eq. (2.13)

$$\left|\vec{L}_{z_{Beam}}\right| = \left|\vec{L}_z\right| = \frac{\kappa\rho}{2c} l|\psi|^2 \tag{2.26}$$

For the spiral initially, as no external forces or torques are considered

$$\vec{L}_{z_{Spiral}} = 0$$

Being

$$\sum \vec{L}_{z_{afterSpiral}} = \vec{L}_{z_{Spiral}} + \vec{L}_{z_{Beam}} = 0 + \vec{L}_z \tag{2.27}$$

Nevertheless, conservation of angular momentum states that:

$$\sum \vec{L}_{z_{beforeSpiral}} = \sum \vec{L}_{z_{afterSpiral}} \tag{2.28}$$

$$\sum \vec{L}_{z_{beforeSpiral}} = 0 \Longrightarrow \sum \vec{L}_{z_{afterSpiral}} = 0$$

Thus, recalling Third Newton's law, the spiral has gained the beam's opposite angular momentum:

$$\vec{L}_{z_{Spiral}} = -\vec{L}_{z_{Beam}} = -\vec{L}_z \tag{2.29}$$

2.7 Rotation of the spiral. Steady Rotation

It is clear now, that the spiral has orbital angular momentum. Being its variation rate positive

$$\vec{L}_{z_{Spiral}} = -\vec{L}_{z_{Beam}} = -\vec{L}_z$$

$$\frac{\mathrm{d}\vec{L}_{z_{Spiral}}}{\mathrm{dt}} > 0 \tag{2.30}$$

The time derivative of angular momentum is torque Γ and it is equal to the sum of the torques exerted on the spiral:

$$\frac{\mathrm{d}\vec{L}_{z_{Spiral}}}{\mathrm{dt}} = \sum \vec{\Gamma}_{Spiral} \tag{2.31}$$

Analyzing the steady rotation of the spiral, one can state three different torques:

- $\vec{\Gamma}_{radiation}$ due to wave propagating through the disk. It has been shown that axial torques exerted by and acoustic vortex on axisymmetric objects can be expressed as [4]:

$$\vec{\Gamma}_z = \frac{1}{\omega}\, l\, P_{abs} \tag{2.32}$$

where ω is the angular frequency of the beam, l the topological charge and P_{abs} the acoustic power absorbed by the object.

P_{abs} can be related with the total acoustic power of the beam $P_{acoustic}$. This linear relation varies depending on the absorptive properties of the material: $P_{abs} = \alpha P_{acoustic}$ with $\alpha \in [0,1]$. Following this lines, $\vec{\Gamma}_{radiation}$ is defined as:

$$\vec{\Gamma}_{radiation} = \beta l \mathrm{P}_{acoustic} \tag{2.33}$$

With $\beta = \frac{\alpha}{\omega}$.

- $\vec{\Gamma}_{solid\ friction}$ exerted by the friction effects between the spiral and the liquids.
- $\vec{\Gamma}_{viscous}$ that states due to dealing with Newtonian's fluids. A rotational viscosity coefficient (μ) results from a coupling between the fluid flow and the rotation of the spiral (Ω_z).

$$\vec{\Gamma}_{viscous} = -\mu\Omega_z \tag{2.34}$$

$$\sum \vec{\Gamma}_{Spiral} = \vec{\Gamma}_{radiation} + \vec{\Gamma}_{solid\ friction} + \vec{\Gamma}_{viscous} \tag{2.35}$$

Considering these equivalences and knowing that the angular momentum can be expressed as the product of the spiral's momentum of inertia I and its angular velocity Ω_z:

$$L_{z_{Spiral}} = I\Omega_z$$

$$\frac{\mathrm{d}\vec{\mathrm{L}}_{\mathrm{spiral}}}{\mathrm{dt}} = \mathrm{I}\frac{\mathrm{d}\Omega_{\mathrm{z}}}{\mathrm{dt}} = \sum \Gamma_{\boldsymbol{Spiral}} = \beta l \mathrm{P}_{\boldsymbol{acoustic}} + \Gamma_{\boldsymbol{solid\ friction}} - \mu\Omega_z \tag{2.36}$$

Being $\frac{\mathrm{d}\Omega_{\mathrm{z}}}{\mathrm{dt}} = 0$ due to steady state rotation

$$\Omega_{\mathrm{z}} = \frac{\beta l \mathrm{P}_{acoustic}}{\mu} - \frac{\Gamma_{solid\ friction}}{\mu} \tag{2.37}$$

With this equation, the existence of rotation in the spiral due to OAM exchange has been demonstrated.

If one assumes no friction effects $\vec{\Gamma}_{solid\ friction} = 0$

$$\Omega_{\mathrm{z}} = \frac{\beta l \mathrm{P}_{acoustic}}{\mu} \tag{2.38}$$

These last two equations state also that the spiral's rotation is closely related with the acoustic power of the beam. Furthermore, they imply that the angular velocity of the spiral $\Omega_{\mathrm{z}}$is directly proportional to the topological charge of the beam.

2.8 Acoustic rotational streaming.

Although acoustic propagation in fluids is normally considered as non-dissipative, dissipation actually occurs as an unavoidable consequence of viscosity and heat conduction [11]. Acoustic attenuation is well known to trigger an axial steady flow usually called acoustic streaming due to the transfer of linear momentum from a progressive acoustic wave to a sound absorbing fluid [12]. When an acoustic vortex is present, its attenuation by the fluid itself is expect to result not only in usual acoustic axial streaming but also in its rotational counterpart called "acoustic rotational streaming" triggered by the radiation torque exerted on the fluid bulk as a result of acoustic OAM transfer to it [13].

As the liquid absorbs part of the acoustic momentum, it is translated into a bulk force field, so it flows. The transfer of linear momentum induces an (principally) axial flow close to the focus (any beam "pushes" the absorbing liquid), whereas the transfer of angular orbital momentum induces an azimuthal flow (an AV beam "twists" the absorbing liquid). In order to evaluate the magnitude of the liquid flow, we model the flow as follows [15]. First, one notes that, due to the impermeability of the disk, the axial flow (hence radial flow as a consequence of mass conservation) is weak in the vicinity of both sides of the disk: This allows to consider a purely azimuthal flow close to the disk. Second, since the disk is located on the transducer focus the bulk field force exerted by the beam on the liquid is locally z-invariant. This allows one to assume a steady, z invariant azimuthal flow close to the disk: $\vec{u} = u_\varphi(r)e_\varphi$. The azimuthal component of the Navier-Stokes equation in cylindrical coordinates satisfies

$$\eta\left(\frac{\partial^2 u_\varphi}{\partial r^2} + \frac{1}{r}\frac{\partial u_\varphi}{\partial r} - \frac{u_\varphi}{r^2}\right) = -f_\varphi, \tag{2.39}$$

Where η is the viscosity of the liquid and $f = \frac{dF}{dV}$ is the external force per volume element exerted on the liquid. The left hand side can be rewritten as

$$\eta\frac{1}{r^2}\frac{\partial}{\partial r}\left(r^3\frac{\partial}{\partial r}\frac{u_\varphi}{r}\right) = -f_\varphi$$

$$\rightarrow\ r^3\frac{\partial}{\partial r}\frac{u_\varphi}{r} = -\frac{1}{\eta}\int f_\varphi r'^2 dr' \rightarrow u_\varphi = -\frac{r}{\eta}\int\frac{dr}{r^3}\left[\int f_\varphi r'^2 dr'\right]. \tag{2.40}$$

f_φ can be expressed as

$$f_\varphi = \frac{\gamma_z}{r}, \tag{2.41}$$

where $\gamma_z = \frac{d\Gamma}{dV}$ is the external torque density exerted on the liquid along the z axis. Let α be the sound absorption coefficient of the liquid. The angular momentum density dL_z that is transferred from the sound wave to a fluid differential particle with height dz is

$$dL_z = L_z(z) - L_z(z+dz) = L_z(z)(1 - e^{-\alpha dz}), \tag{2.42}$$

Since $\alpha dz \ll 1$,

$$dL_z = L_z[1 - (1 - \alpha dz)] = \alpha L_z dz. \tag{2.43}$$

Combining equations, one has

$$\gamma_z = \frac{dL_z}{dt} = \frac{dL_z}{dz}\frac{dz}{dt} = \frac{dL_z}{dz}c = c\alpha L_z \tag{2.44}$$

With eq. (2.41) to replace $f_\varphi$in eq. (2.40) and obtain

$$\rightarrow u_\varphi = -\frac{c\alpha}{\eta} r \int \frac{dr}{r^3}\left[\int \frac{dL_z}{dV} r' dr'\right]. \tag{2.45}$$

The angular momentum density of the sound wave yields

$$\rightarrow u_\varphi = \frac{\alpha}{2\omega\rho c\eta} r \int \frac{dr}{r^3}[\int p^* p\, r' dr'] \tag{2.46}$$

Within the approximation (2.7)

$$\rightarrow u_\varphi = \frac{\alpha\omega_0 p_0^2}{2\omega\rho c\eta} x \int \frac{dx}{x^3}\left[\int x'^2 e^{-2x'^2}\, x' dx'\right] \tag{2.45}$$

Integration and evaluation in the boundary conditions $u_\varphi(\infty) < \infty$ and $u_\varphi(0) = 0$ yields

$$\rightarrow u_\varphi = \frac{3\alpha\omega_0 p_0^2}{2\omega\rho c\eta}\frac{1-e^{-2x^2}}{16x}. \tag{2.46}$$

In this case (positive l), $u_\varphi$is negative for all x. The absorption coefficient α may be expressed in terms of the viscosity

$$\alpha = \frac{2\omega^2}{3\rho c^3}\left(\eta + \frac{3}{4}\eta_B\right) \qquad if \qquad \frac{\omega}{\rho c^2}\left(\frac{4}{3}\eta + \eta_B\right) \ll 1, \tag{2.47}$$

Where $\eta_B$is the bulk viscosity [13]. Combining it with eq. (2.46) to eliminate α yields

$$\Rightarrow u_\varphi(x) = -\frac{\omega\omega_0 p_0^2}{\rho^2 c^4}\left(1 + \frac{3\eta_B}{4\eta}\right)\frac{1-e^{-2x^2}}{16x}. \tag{2.48}$$

The angular velocity of the liquid flow is

$$\Omega_{flow}(x) = e_z \frac{u_\varphi(x)}{r(x)} = e_z \frac{u_\varphi(x)}{\omega_0 x} = -e_z \frac{\omega p_0^2}{16\rho^2 c^4}\left(1 + \frac{3\eta_B}{4\eta}\right)\frac{1-e^{-2x^2}}{x}. \tag{2.50}$$

Note that u_φ and Ω_{flow} depend only on the ratio η_B/η and not on the absolute values. This result provides the existence of a stream generated by the action of the vortex over the fluid. It has been observed in previous works [15] that on the focal position dust particles and bubbles are rotating following this pattern.

This theory sustains the experiments that will be developed and explained in the following chapters.

2.9 References

[1] F. Pampaloni, J. Enderlein. Gaussian Hermite- Gaussian and Laguerre- Gaussian Beams: A primer. EMBL Cell Biology and Biophysics. (2004)

[2]J. F. Nye, M. V. Berry. Dislocations in wave trains. Proc. R. Soc. London. A. 336, (1974)

[3]J. L. Thomas, T. Brunet. F. Coulouvrat. Generalization of helicoidal beams for short pulses. Phys. Rev. E 81, 016601 (2010).

[4] L. Zhang and P. Marston. Angular momentum flux of nonparaxial acoustic vortex beams and torques on axisymmetric objects. Phy. Rev E 84, 065601 (R) (2011).

[5] J. Lekner. Acoustic beams with angular momentum. J. Acoust. Soc. Am. 120 (6)(2006).

[76] L.E. Kinsler, A. R. Frey, A. B. Coppens and J.V. Sanders, Fundamentals of Acoustics (2000) John Wiley & Sons.

[7] Cohen-Tannoudji, Claude; Diu, Bernard; Laloë, Franck. Quantum Mechanics. (2006). John Wiley & Sons.

[8] Likins, Peter W., Elements of Engineering Mechanics. (1973). McGraw-Hill Book Company.

[9] Fowles, G. R.; Cassiday, G. L., Analytical Mechanics. 6th Ed. Saunders College (1999). Publishing.

[10] Serway, R. A. and Jewett, Jr. J. W., Physics for Scientists and Engineers. 6th Ed. Brooks Cole (2003).

[11] P. M Morse, K.U. Ingard. Theoretical Acoustics. Princeton University (1968).

[12] M. F. Hmilton, D. T. Blackstock. Nonlinear acoustics. Academic (1997).

[13] A. Anhäuser, R. Wunenburger, E: Brasselet. Acoustic rotational manipulation using orbital angular momentum transfer. Phy. Rev. Let. 109, 034301 (2012)

[14] C. Escobar. Acoustic rotor. Driving rotation through acoustic vortex creation and exchange of orbital angular momentum. Université Pierre et Marie Curie. (2013)

[15] A. Anhäuser. Rotation, twist and flow induced by an intense acoustic vortex beam. Université Bordeaux 1. (2011).

Chapter 3

Experimental Procedure

As it was mentioned before, during this work two main experiments concerning acoustic vortices and orbital angular momentum transfer were studied. Though both experiments share common elements and procedures, each experiment will be described independently after a brief description of the experimental elements.

3.1 Main experimental components

a) Acoustic transducer

The regular beam required to create the AV is generated by a sound source with its emitting direction on the z axis. The source of sound used is a focused spherical transducer, whose shape causes a high focalization of the beam in the center of curvature of its surface. This high focalized point is the focus of the transducer, and the horizontal plane (x-y) in which it is located is called the focal plane. The focus is the point of maximum intensity of the beam (Figure1).

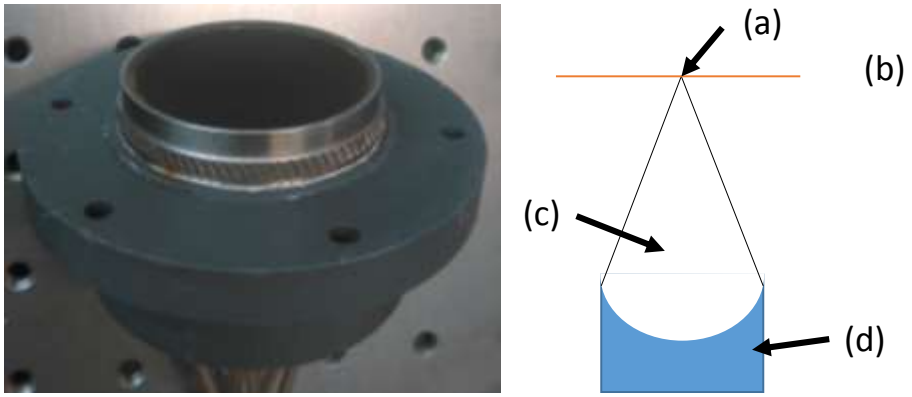

Figure 1. (a) Focus. Point of maximum acoustic intensity of the beam. (b)Focal plane. Perpendicular to the beam axis of propagation z. (c) Focused regular beam. (d) Focused spherical transducer.

This transducer works under the application of a modulated voltage signal to a piezoelectric material, which oscillates at the frequency of the input signal and thus generates an acoustic wave inside a liquid.

In this work we focused on 2 transducers, plane wave transducer working at a frequency of 2.5 MHz and an 8-segment transducer working at a frequency of 2.25 MHz.

b) Hydrophone

A hydrophone is an acoustic pen-like sensor with an active area of 80 µm, which transforms a pressure value measured into an electric current visible on an oscilloscope. The hydrophone is not calibrated so measurements provide only relative values.

Figure 2. Hydrophone

3.2 Rotation Induced by and Intense Acoustic Vortex Beam

The aim of this experiment was to observe the transfer of angular momentum between an acoustic plane wave and a polylactic acid (PLA) disk. This exchange of angular momentum generates and acoustic vortex with a topological charge given by the shape of the disk (figure 3). This transformation of an acoustic plane into an acoustic vortex occurs when the wave passes through matter. The object will be the polymer disk which has a well-defined-θ-variant design responsible of imprinting the wave a phase delay and thus providing an amplitude factor of $e^{il\theta}$.

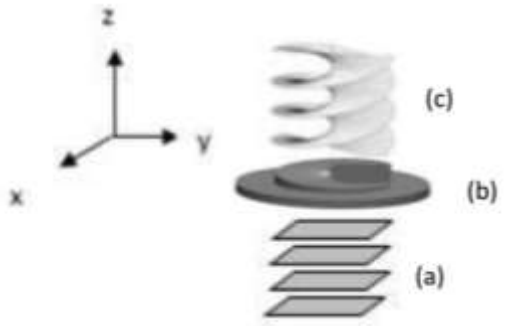

Figure 3. (a) Plane isophase surfaces of an acoustic regular beam emitted by a transducer which direction of propagation is the Z axis. Without azimuthal dependence. (b) Polymer material with spiral shape. Its -θ variant design will cause a phase delay to the wave that trespasses it. (c) Resulting beam after crossing the spiral has become an Acoustic vortex, characterized by its azimuthal dependent amplitude factor $e^{in\theta}$ [1].

To accomplish this experiment, two set ups were assembled; one to characterize the acoustic transducer and another to observe the exchange of orbital angular momentum. In the second set up, few modifications are made in order to observe whether the rotation of the disk (orbital angular momentum exchange) or the generated vortex.

The first set up is shown in figure 4. This set up consists of an acoustic spherical transducer with a radius of 38 mm with a bandwidth of 1.5 to 3.5 MHz immersed in a tank filled with deoxygenated and degasified water. The transducer is connected to a 75 watts CW Amplifier Research amplifier which is supplied with a burst signal provided by a Hewlett Packard arbitrary wave generator at different frequencies between a range of 2.2 MHz to 3.5 MHz. The rate and number of this burst signals is determined by the experiment. For rotation, a high power is required meaning a high burst rate and high number of cycles, always keeping the duty cycle on 20%. On the other hand, when measuring the vortex profile, high power is not required meaning low burst count numbers.

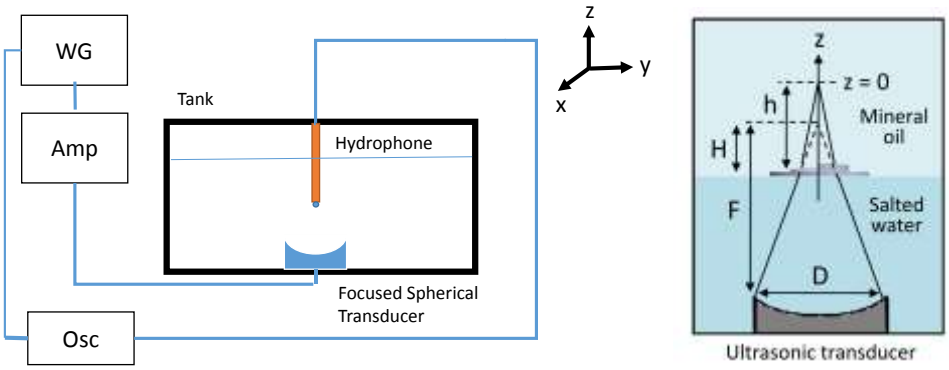

Figure 4. Experimental set up to characterize the acoustic transducer profile and the geometry of the transducer

In this set up, the profile of the transducer at two different frequencies 2.5 and 3.3 MHz was measured. For this mono-element transducer it is supposed that all the points emitted have the same phase and the same amplitude. This means,that the amplitude assigned to each wave coming from the transducer has a profile given as $u(r', \theta') = u_0$. In this case, the integral over θ' gives the function Bessel J_0 of first type and order zero:

$$p(r, z, \theta, t) = A(r, z, t) \int_0^a J_0\left(\frac{krr'}{z_0+h}\right) e^{i\frac{kr'^2}{2}\left(\frac{1}{(z_0+h)}-\frac{1}{z_0}\right)} r' dr' \qquad (3.1)$$

This field equation gives a good description of the pressure field near the center. It can be seen that in the focal plane (h=0) the amplitude has zero values in the zeros of the Bessel function. The amplitude is maximal in the center of the sphere. The obtained measured fields are shown below with their theoretical equivalents.

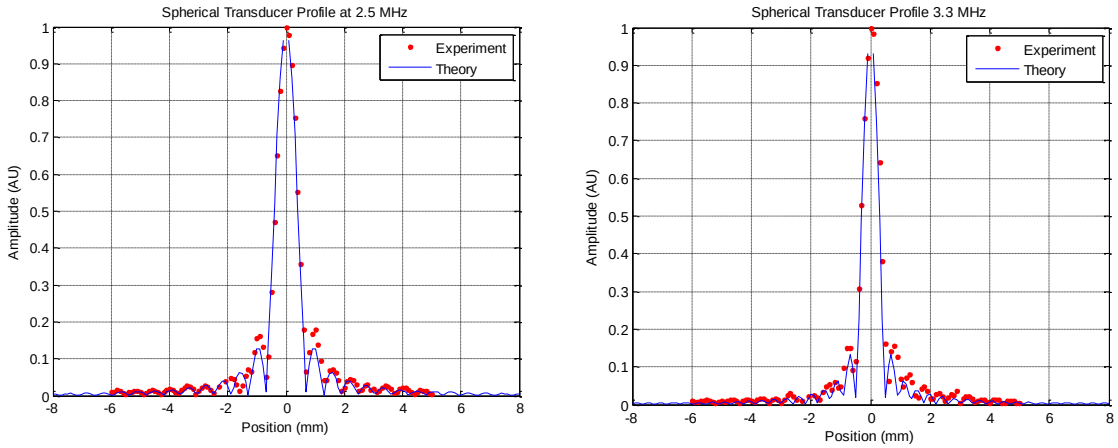

Figure 5. Profile of the transducer along the X axis for two different frequencies.

Once the transducer was verified to have a nice profile as theory predictes, the focal point was searched in order to have the maximum power location to work. This was done by redoing scans along the X, Y and Z axes. These measurements of the relative position of the focal plane also gave information about the symmetry of the profile as can be seen in the figure 6.

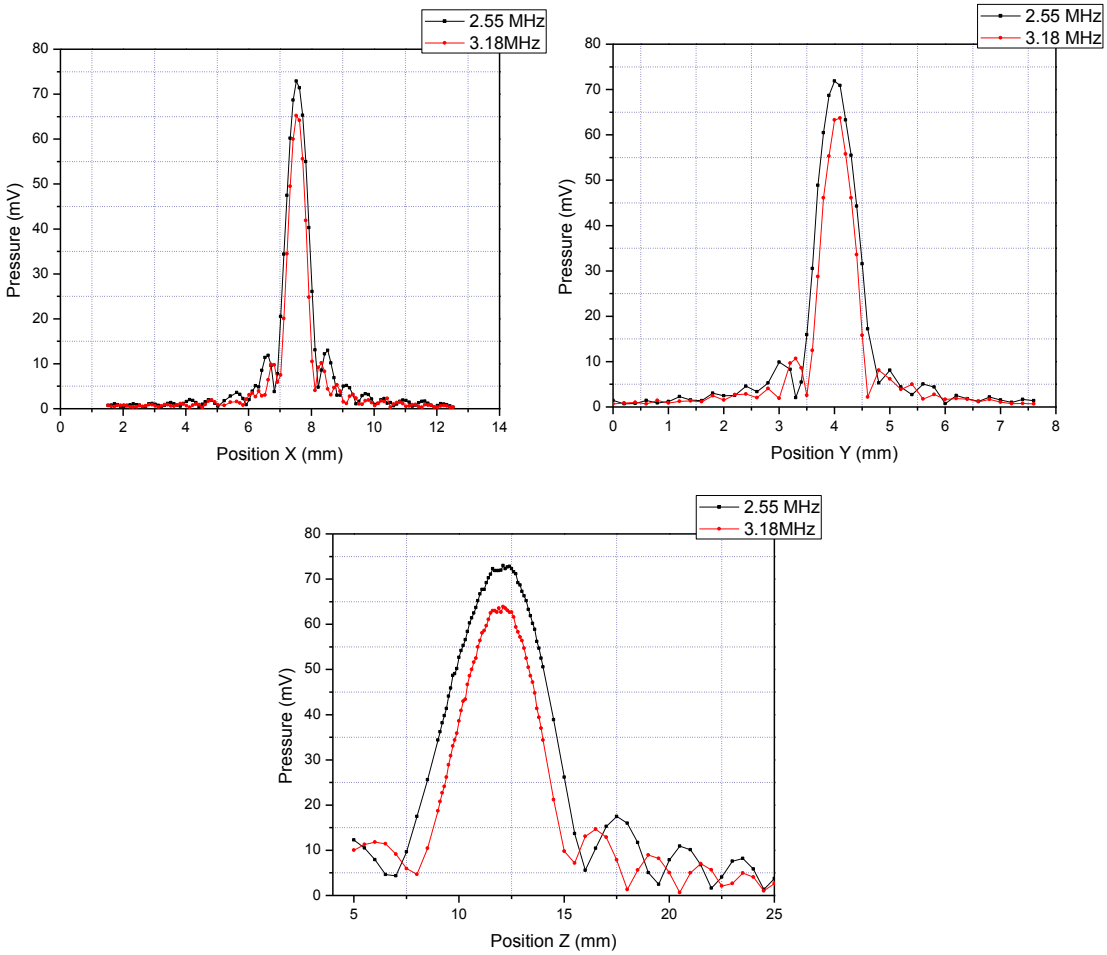

Figure 6. Graphs obtained for the pressure field for the frequencies f=2.55MHz and f=3.18MHz. The response obtained is in agreement with the theory.

Once this characterization of the transducer was done, the set up shown in figure 7 was assembled. The objective of this set up is to observe rotation of a PLA disk due to exchange of momentum. To place the disk at the required height, an interface between two immiscible liquids is generated. This height is located few millimeters below the focal

distance so the PLA disk could absorb the highest amount of acoustical power provided by the transducer.

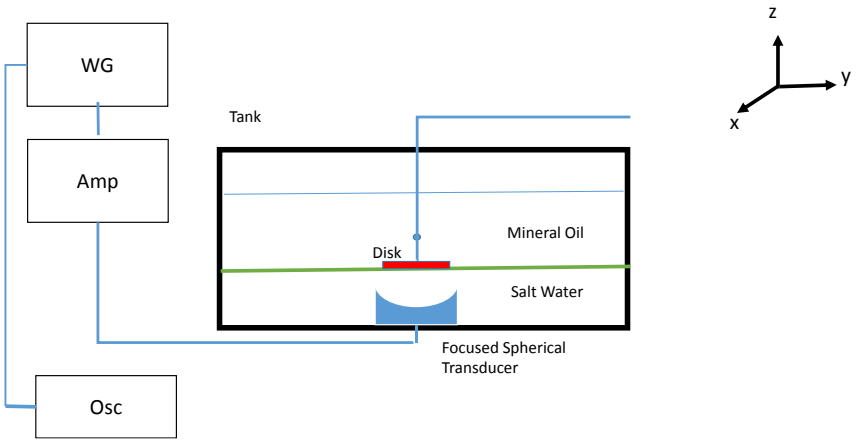

Figure 7. Experimental setup to observe rotation of the disk.

The shape and structure of the disk is designed according to the wanted effect. As it has been exposed above, the main characteristic of an acoustic vortex is that its amplitude has a factor of the form $e^{il\theta}$ where $l \neq 0$. Due to the phase dependence of the azimuth angle θ, these beams carry angular momentum and thus, torque appears leading to rotation. The aim is to obtain a θ-linear dependence in the phase.

To achieve a linear variation of the beam's phase with the azimuth angle, a θ-linear dependence of phase delay has to be applied to the incident beam. The main key factor that leads to phase modulation is the phase difference induced by matter. Wave propagation through the disk results in a beam of the form

$$\psi(r,t) = e^{i(qz-\omega t)} e^{il\theta} A(r) \tag{3.2}$$

where $A(r)$ is the amplitude with only radial dependence. It can be seen that its phase is affected by the sound velocity c in the media. This can be seen as:

$$Incident\ beam\ on\ the\ spiral: l = 0 \xrightarrow{yields} e^{il\theta} = 1$$

$$\psi(r,t) = e^{i(qz-\omega t)} A(r) \tag{3.3}$$

$$K^2 = k^2 + q^2 \tag{3.4}$$

$$K = \frac{\omega}{c} \tag{3.5}$$

Taking this into account, the beam was forced to pass through different media. In this case, the three immiscible liquids with different values of sound velocity c: salty water, polymer (PLA) spiral and finally mineral oil.

Liquid	Phase sound velocity [m/s]
Saturated salty water	2210
Mineral Oil	1462
Polymer (PLA) spiral	1750

The only medium capable of imprint itself a θ-linear dependence of phase delay is the PLA disk. As seen in figure 8, the azimuth angle is a critical parameter of the spiral, and it is linearly related with the thickness of the spiral e. The thickness of the spiral varies with θ value:

$$e = e(\theta) = \frac{e_s \theta}{2\pi} \qquad \theta \in [0,2\pi] \tag{3.6}$$

Figure 8. Phase modulation. Propagation through the spiral [1]

This phase modulation can be explained if the spiral is reshaped as shown in figure 9.

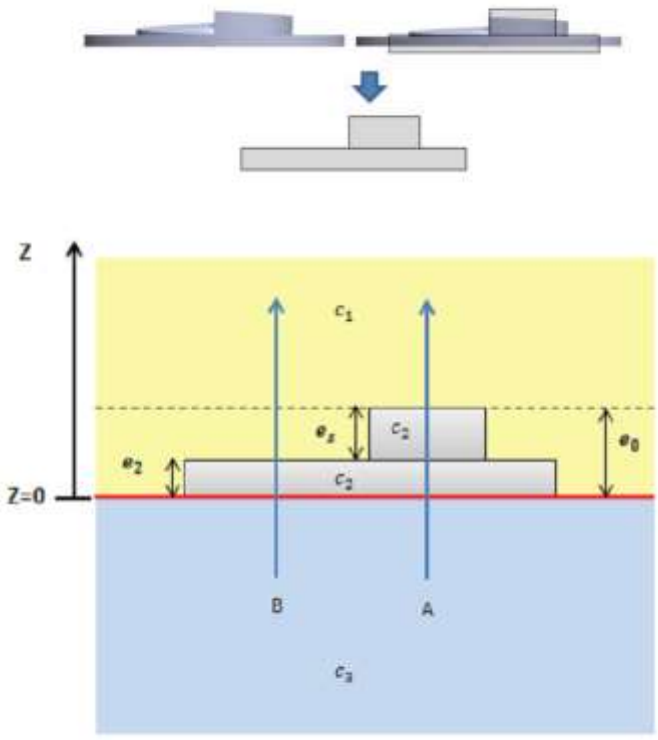

Figure 9. Cross section of the PLA disk (phase sound velocity c2) in between the immiscible liquids. Yellow area represents mineral oil (phase sound velocity c1) and blue area represents salted water (phase sound velocity c3). Blue arrows show the propagation direction of the sound beam across the media. Dotted black line indicates the altitude z where the phase difference was calculated (beginning of the resulting AV beam). (Dimensions: e_0=total height (spiral + basis); e_s= spiral max height; e_2= basis height).[1]

Considering only the spatial dependence of the incident beam before crossing the disk [1]:

$$\psi(r,t) = e^{i\varphi} A(r) \tag{3.6}$$

Being the phase $\varphi(z) = Kz$ (simplifying q to equal to $K = \frac{\omega}{c}$).

The wave emitted by the transducer crosses the spiral in the z axis direction (blue arrows). Due to the thickness variation of the spiral, and thanks to the fact that the phase velocities are different in both media, a phase shift is generated.

$$\text{B: } \varphi(e_0) - \varphi(0) = \frac{\omega}{c_2} e_2 + \frac{\omega}{c_1}(e_0 - e_2) \tag{3.7}$$

$$\text{A: } \varphi(e_0) - \varphi(0) = \frac{\omega}{c_2} e_0 \tag{3.8}$$

$$\Delta\varphi = \Delta\varphi_B - \Delta\varphi_A = \omega(e_0 - e_2)\left(\frac{1}{c_1} - \frac{1}{c_2}\right); \qquad (e_0 - e_2) = e_s \tag{3.9}$$

Here stands that the phase difference has become a function of the thickness of the disk e. Therefore, function of the azimuth angle θ. As one of the requirements is that the phase factor $e^{il\theta}$ is periodic, the phase difference between waves must satisfy:

$$\Delta\varphi = \Delta\varphi_B - \Delta\varphi_A = \omega e_s \left(\frac{1}{c_1} - \frac{1}{c_2}\right) = n2\pi \tag{3.10}$$

This allows to determine the maximum spiral's thickness:

$$e_S = \frac{\frac{n2\pi}{\omega}}{\left(\frac{1}{c_1} - \frac{1}{c_2}\right)} \tag{3.11}$$

Even though a variety of spirals with different topological charges were available, only one with a topological charge of $l = 4$ was chosen to work. The number of ramps imprinted in each spiral indicates the value of the topological charge of the AV. For this specific spiral one have:

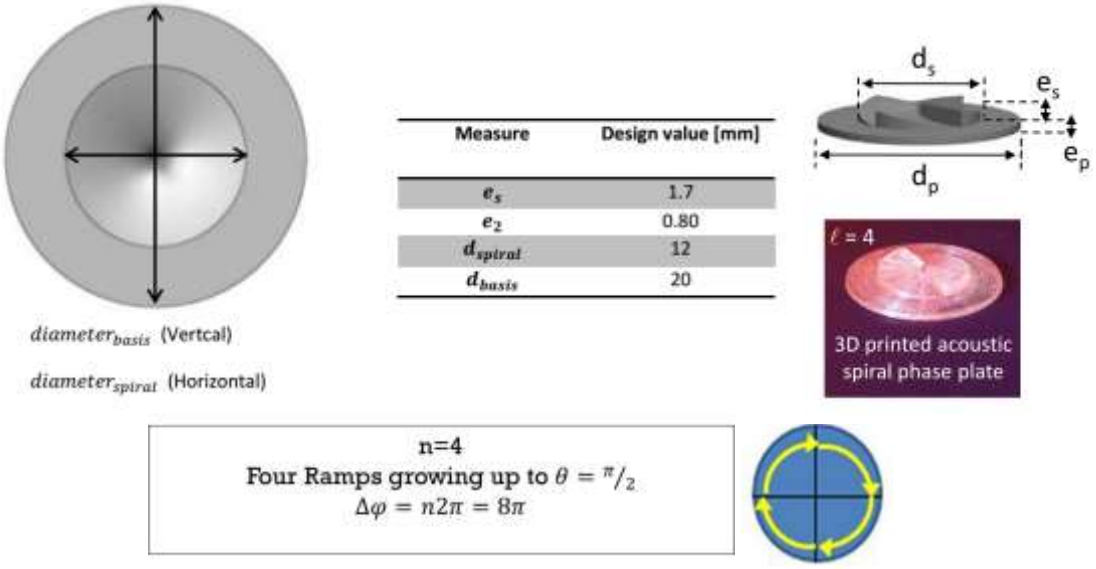

Figure 10. Ramp design for the spiral with topological charge of $l = 4$ and its respective phase difference value. Yellow lines indicate the progression of $e = 0$ up to $= e_s$ [1].

To place the spiral over the transducer and to keep it fixed to the position with freedom of rotation, a needle is used. The tip of this needle is placed in a small hole located at the center of the spiral. The hole has the size required to hold the needle but not to cause friction between the 2 elements.

Once the set up was ready, one proceeded to measure the angular velocity of the disk under the influence of the transducer. It was important to verify that no air bubbles were present below or above the spiral because they interact with the wave and alter the expected result. Using a chronometer, the angular sound velocity of the spiral was measured at different input voltages to observe its response. At first only the two frequencies previously mentioned were used but over the experiment few modifications were done and will be diskussed in the following chapter

As mentioned before, this experiment is divided in two parts, the observation of exchange of angular momentum and the verification of the existence of the acoustic vortex. To achieve the latter a pressure measurement of the downstream beam, across the spiral was taken. For its accomplishment, there is a need of cancelling the rotation effect previously described. This means, create a stationary scenario that allows capturing the AV pressure map. These AV pressure map have a very specific profile.

To obtain the stationary state, the spiral was fixed to a block-guide previously built [Fig.11].

Figure 11. Diagram of the free spiral/Fixing block-guide. It is formed by two holes, the big one is for introducing the spiral as shown by the blue arrow. The small one is for holding and positioning it in the experimental set up [1].

During this second part the set up was re-arranged to perform a full profile scan over the X-Y plane as follows:

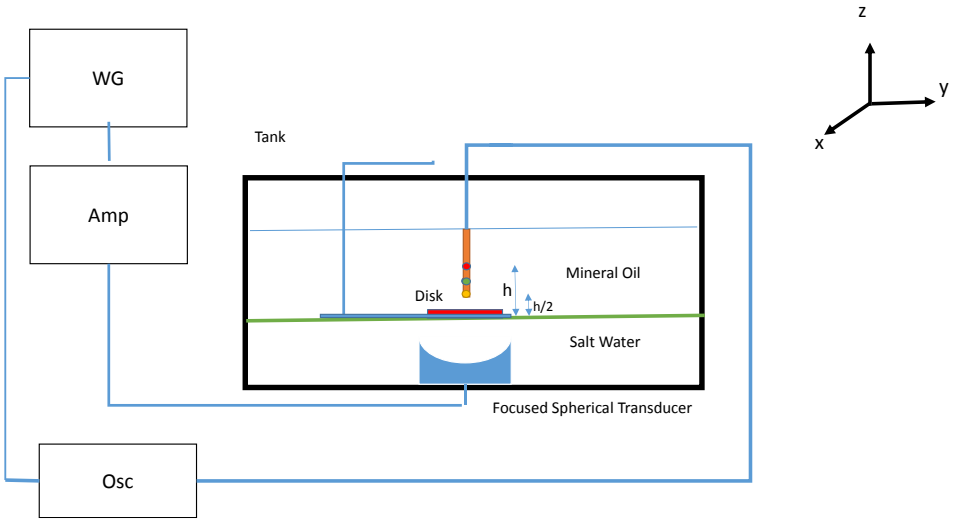

Figure 12. Experimental setup used to measure the acoustic pressure field.

In this case, a resolution of 300 µm was used to reproduce the vortex profile.

A wave function generator (WG) provides an electrical signal to the transducer. This signal was previously amplified by the amplifier (AMP). The transducer is driven at 200 mVpp amplitude with the two frequencies previously mentioned in wave trains of 20 cycles with a rate of 1 KHz, as lower powers are required now. Just like the case of the characterization of the transducer, a hydrophone ONDA is used, having three degrees of freedom along the X, Y and Z axis. This element sends an electric signal to the oscilloscope which is proportional to the sound pressure at the sensor location.

Due to the change of media between water and oil, the focal distance of the transducer is now displaced a few millimeters above its original positions. This new position of the focal plane was found theoretically and experimentally and it will be shown in the next chapter.

3.3 Acoustic Rotational Streaming

The second part of this work is related to the transfer of angular momentum from an acoustic vortex with topological charge to a liquid, phenomenon known as acoustic rotational streaming. As mentioned above, the main elements of the previous experiment remain, with the difference that now an eight segment spherical transducer (Imasonic 7592

A101) was used. Just as in the previous experiment, the transducer is submerged inside a tank filled with degasified and demineralized water.

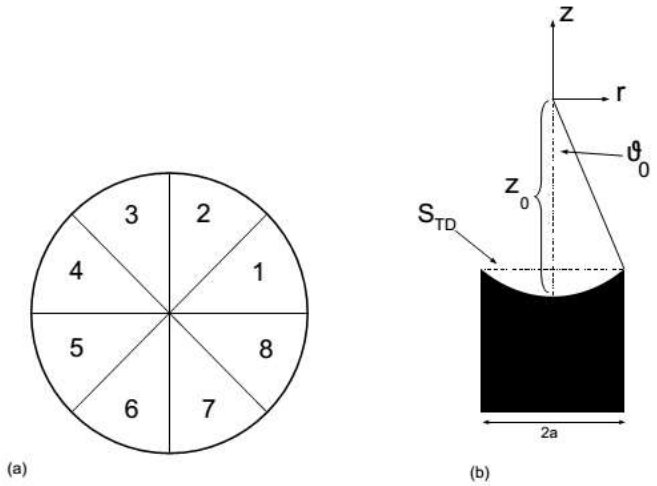

Figure 13. a) Spherical transducer divided into eight elements viewed from the top. B) Geometrics of the transducer where z0 represents the focal disntance, r the radius of the transducer, $\vartheta_0$the angle formed by the z axis and the vector who goes from the border of the transducer to the focal point. [2].

This transducer was driven at 2.25 MHz only, in wave trains of 20 to 300 cycles duration. Each segment of the transducer can be driven independently. An electrical circuit ensures that each transducer element receives the signal with the appropriate phase shift to create an AV. Each of the T/4 and T/8 delay cells in the circuit can be activated independently where T is the period fo time required. This enables to crate charges ±1, ±2, ±3 by activating the phase shift cells and connecting the transducer elements properly.

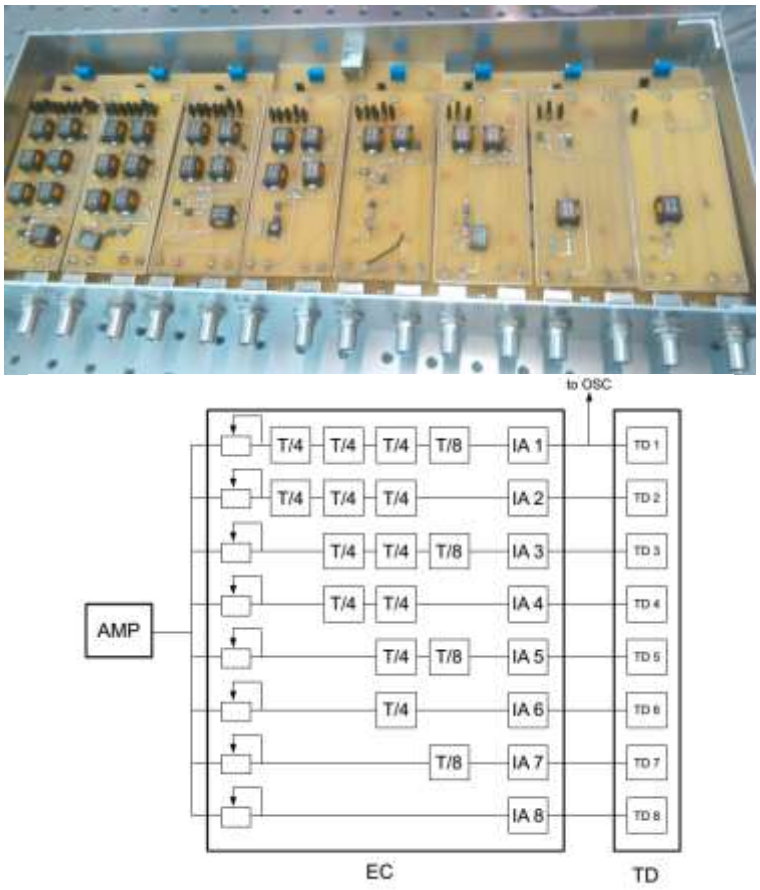

Figure 14. Electronic circuit responsible to introduce the phase difference between segments and its corresponding diagram [2].

The system was fed with a 200 mVpp signal at 2.25 MHz provided by a function generator and amplified. To obtain the pressure profile of the beam, a scan was done along the X and Y directions with the hydrophone. The hydrophone is able to move in the XYZ directions as shown in figure 15.

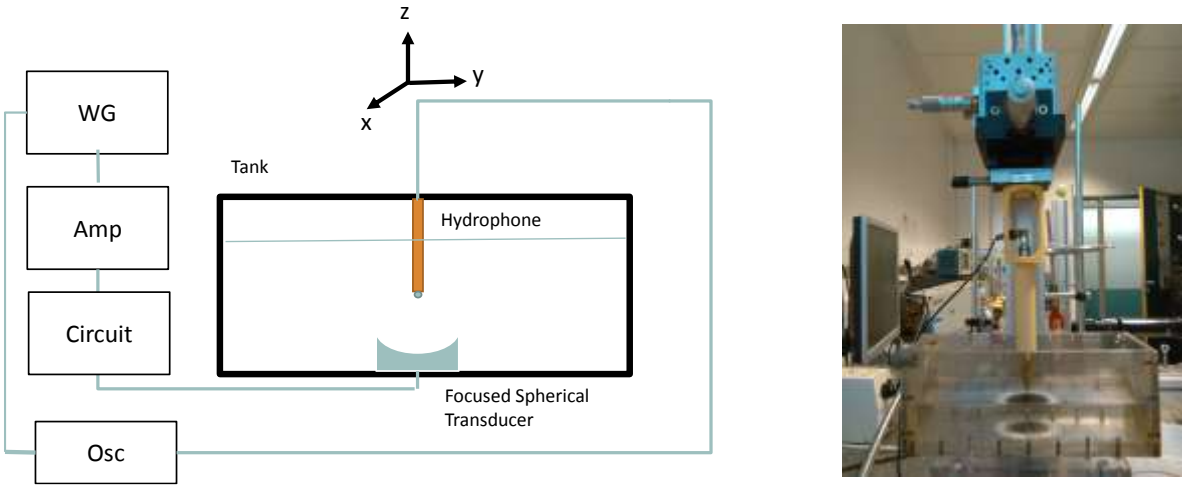

Figure 15. Experimental Setup

To locate the focal position of this transducer, three scans were done along the three axis (X, Y and Z) with a resolution of 200 µm without the phase delay system. The resultant profiles are observed in figure 16.

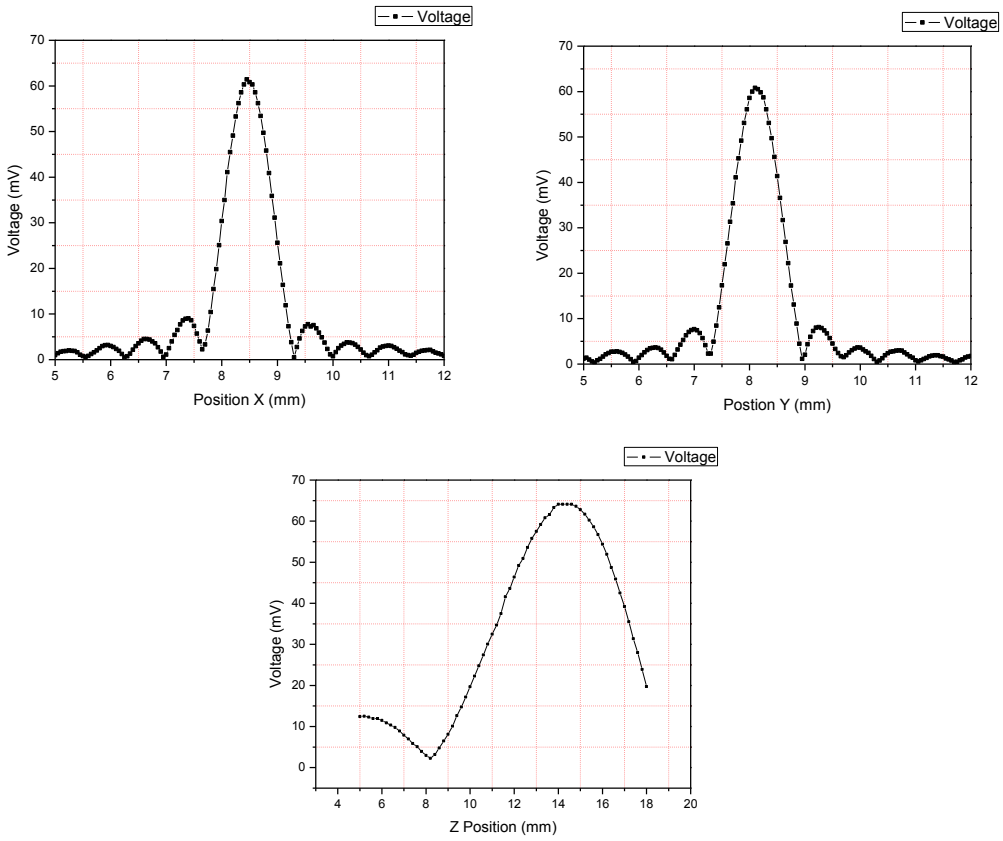

Figure 16. Pressure profiles of the transducer without the phase delay between each segment along the axis X, Y and Z

As expected, the transducer worked nicely without the phase delay. The focal plane was found to be 38 mm above the surface of the transducer. Once this was done, the phase delay system was introduced and the profile and phase of the helical beam were measured.

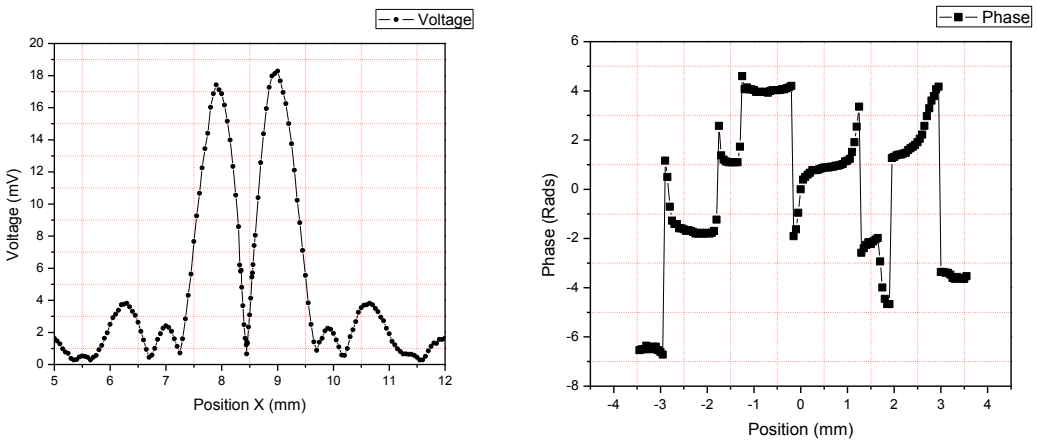

Figure 17. Pressure profile of the donut in the X axis and phase of the helical beam. The position in the phase corresponds to the center of the donut

It can be seen that the system behaved as expected with a nice singularity in the center of the profile. It is also possible to observe the phase change by π between two opposite positions along the axis. The corresponding wavelength of the sound waves generated by the transducer at this frequency in water turns to be $\lambda = 660\ \mu m$. The radius of the donut is around 1 mm.

With the transducer and phase delay system working, the set up was changed to observe the acoustical rotational streaming. For this purpose, a container called Opticell was used. An opticell is a cell culture system. It combines two parallel gas permeable, cell culture-treated polystyrene membranes with a thickness of 75µm and positioned 2 mm apart each other. This cell allows 10 ml of volume. The new set-up is shown in figure 18.

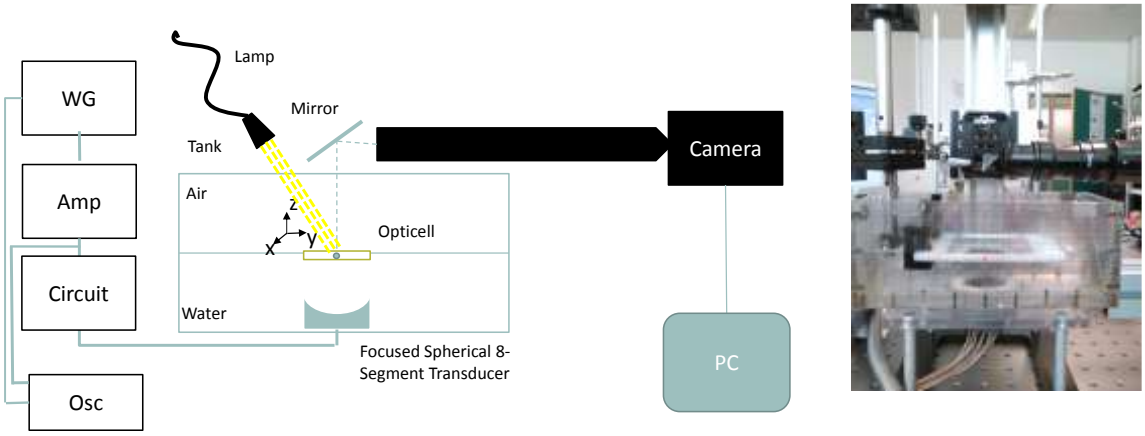

Figure 18. Experimental set-up to observe rotational streaming.

In this experiment, PMMA particles with a 6 µm diameter are used as tracers inside the opticell. The opticell is located on the focal plane of the 8 segment transducer. The phase delay system is fed with a 2.25 MHz and 200 mVpp signal with a burst count of 450 cycles and a burst rate of 1 KHz. The point of using the opticell is to generate a standing wave along the Z axis of the transducer and to generate a flow inside the opticell, where the propagating wave and the reflected wave cancel their linear momentum but the angular component of the field duplicates its value. This generates a stream inside the opticell, moving the PMMA tracers with it. To observe the movement of the tracers, a Photron SA5 fastcam captures 50 frames per second of the particles.

Once the particles were trapped and the phenomenon observed, the characterization of the system and some properties were analyzed, this will be explained in the next chapter.

3.4 References

[1] C. Escobar. Acoustic rotor. Driving rotation through acoustic vortex creation and exchange of orbital angular momentum. Université Pierre et Marie Curie. (2013).

[2] A. Anhäuser. Création et étude d'un vortex acoustique à l'aide d'un transducteur sphérique. Centro de Physique Moléculaire Optique et Hertzienne à Bordeaux. (2010)

Chapter 4

Results

In the previous chapter, the experimental set ups involved in this were presented. In this chapter, the results and modifications done over the experiment will be treated.

4.1 Rotation Induced by an Intense Acoustic Vortex Beam

Using the set up shown in figure 7 of the previous chapter the rotation of the spiral due to transfer of angular momentum was observed. The first case was observed at a frequency of 3.3 MHz. This frequency was chosen as result of the following equation

$$f = \frac{1}{\epsilon\left(c_1^{-1} - c_2^{-1}\right)} = 3.31\ MHz \tag{4.1}$$

With $\epsilon = 1.7mm$ is the thickness of the disk, $c_1 = 1.460\ Km/s$ is the sound speed in the mineral oil, $c_2 = 1.970\ Km/s$ is the sound speed in plastic.

The angular velocity was obtained by measuring the time it took the disk to give a whole turn around its axis. This was done using a chronometer. Many factors are involved in the rotation of the disk such as: bubbles, dirt, dust, temperature gradient, etc., so the data obtained is not easily reproduced. The signal was applied at 200 mVpp amplitude and a frequency of $f = 3.3MHz$, a burst rate of $1.0\ KHz$ with 660 cycles to get a 20% of duty cycle. It is important to mention that the position of the disk given by the interface between water and oil is selected in such a way that the most part of the power provided by the transducer reaches the bottom of the spiral as shown in figure 1.

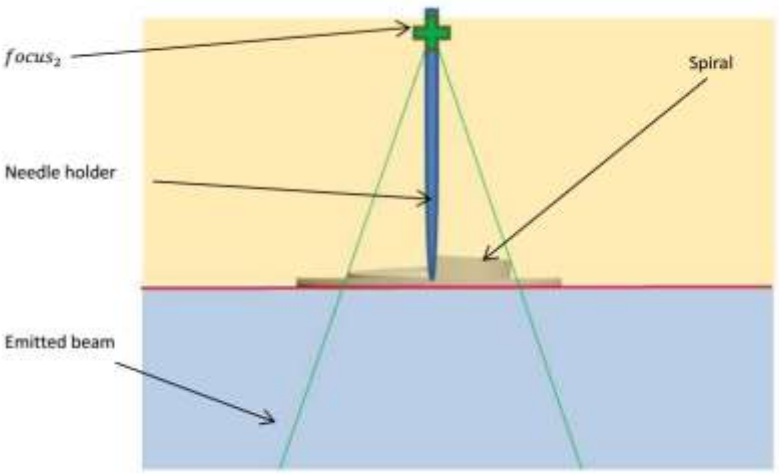

Figure 1. Transverse profile of the spiral and the hold needle.

Once the optimal position was found, two measurements of angular velocity VS voltage were done.

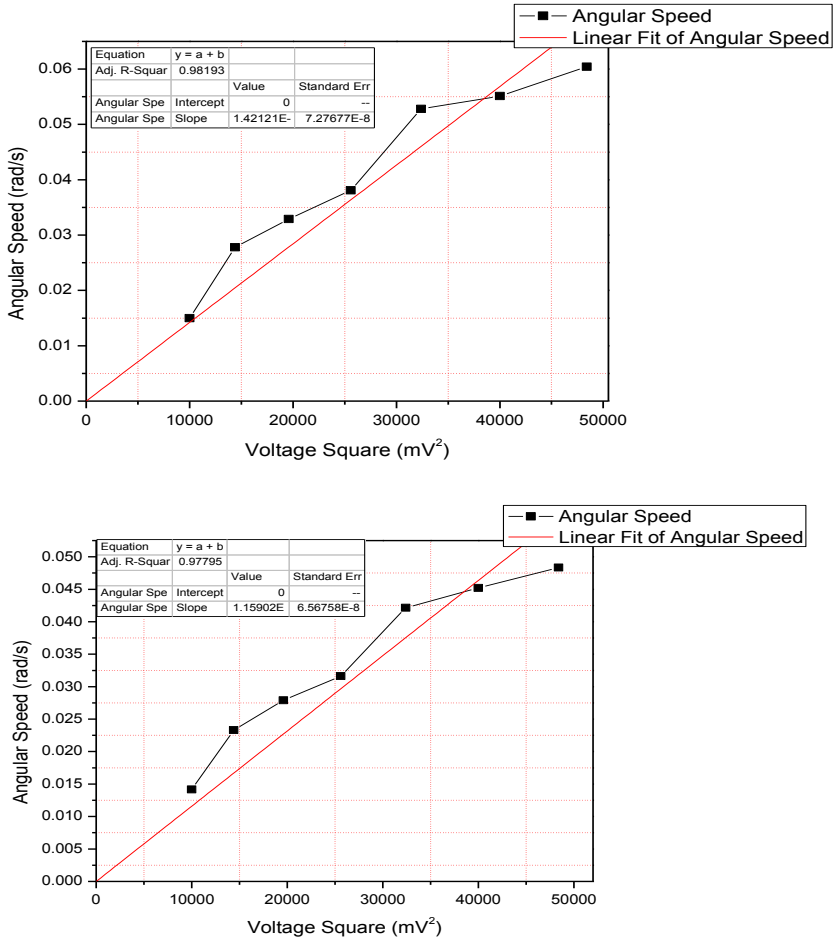

Figure 2. Graphs obtained for Angular Velocity (Ω) VS Voltage square (V^2)

In these graphs one can see that the system presents an almost linear response, showing the presence of solid friction. Solid friction refers to that due to the movement of a solid inside a liquid. This solid friction can be consequence of different factors. The red line represents the data fitting and the black line represents the expected response. Once the measurement of angular rotation was done, one proceeded to obtain the pressure profile of the vortex recalling the modifications to the experimental set up mentioned on the previous chapter.

To achieve this, the disk was fixed to a block guide in order to cancel the rotation effect, and thus create and stationary scenario that allows capturing the AV pressure map.

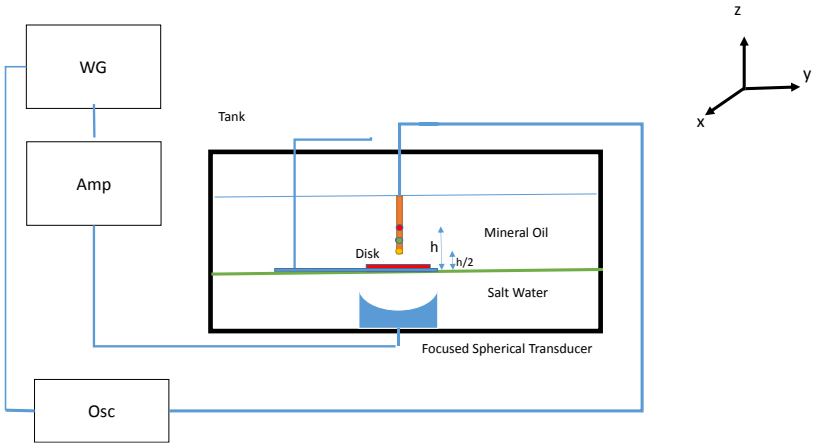

Figure 3. Experimental setup used to measure the acoustic pressure field.

The distance h is the position of the new focus,measured from the interface. In order to find this new position, a small geometrical calculation can be done.

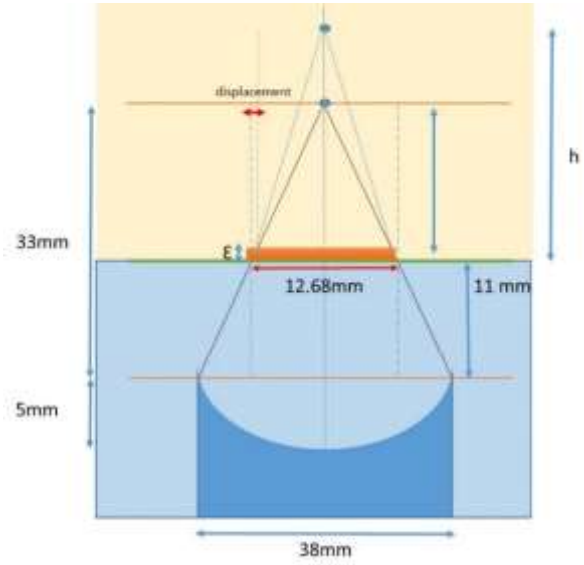

Figure 4. Geometric scheme.

Using the distances between the elements and the Snell's law for refraction in media, an approximate value of h can be obtained. Using the first triangle made by the focus, the radius of the spherical transducer and the distance from the border of the transducer and the focus, one can get the incident angle θ_i. Thanks to triangles equality, ones has the incident angle necessary for the Snell's law. Applying the Snell's law to the surface, the angle of refraction is obtained. Using this angle inside the disk, allows one to know the displacement inside the disk. With this new position over the disk, one can apply trigonometric functions to find the position of h. Using the values:

C water=1783 m/s;

C plastic=1970 m/s;

C oil=1460 m/s

$$\theta_i = \arctan\left(\frac{19mm}{33mm}\right) \tag{4.2}$$

$$\beta = \arcsin\left(\frac{1460}{1783}\sin\theta_i\right) \tag{4.3}$$

$$displacement = \epsilon tan\left(arcsin\left(\frac{1783}{1970}sin\theta_i\right)\right) \tag{4.4}$$

$$h = \frac{6.34 - displacement}{tan\beta} \tag{4.5}$$

The calculated value for h is **h= 12.2409 mm**.

Once this value is known, the hydrophone is placed at a distance $\frac{h}{2} \approx 6.12mm \sim 6.5mm$ from the disk so a good scan over the XY plane could be done.

In order to verify this value, a quick scan over the Z axis was done to observe the behavior of the generated vortex. In theory, as one approaches the focus, the distance between two maximum points should decrease and after the focal point this distance grows. The transducer was driven at 200 mVpp amplitude and a frequency $f = 3.30MHz$ in wave trains of 25 cycles and 100 Hz rate. As an example, here are 3 different graphs showing this behavior:

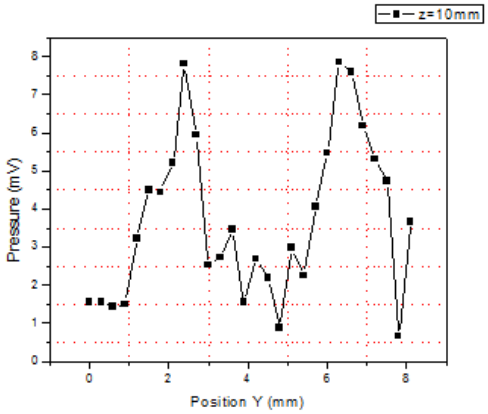

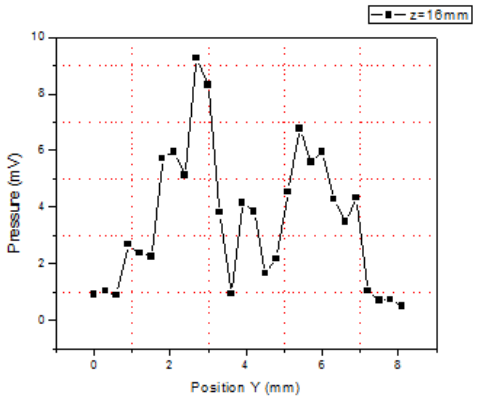

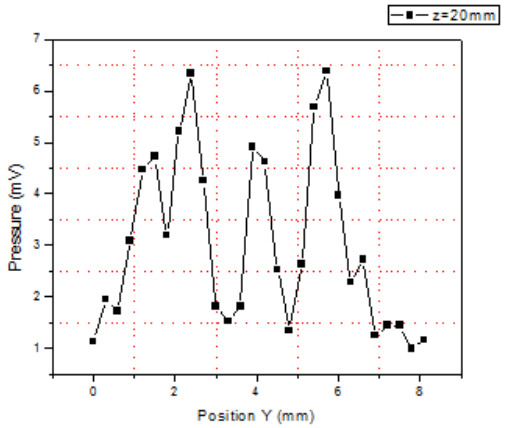

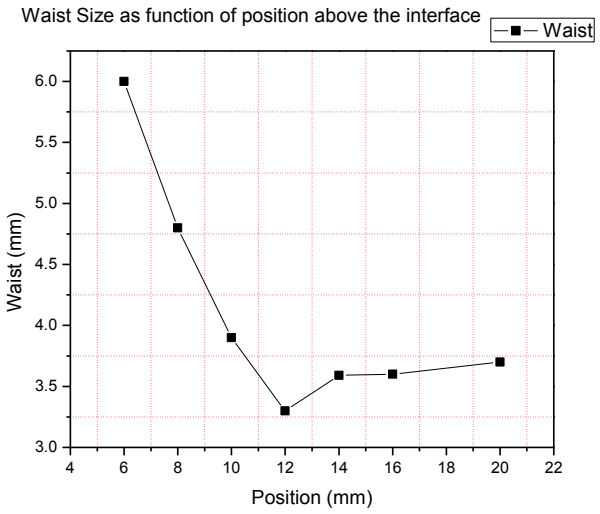

Figure 5. Graphs for the Y Scan for different values of Z.

Even when the resolution is not the best one can observe from the obtained results that the value of h is within an acceptable range and it was possible to continue with the measurements of pressure.

As now the intensity of the pressure field was not relevant, new parameters for the transducer were used. The transducer was driven at 200 mVpp amplitude and a frequency of $f = 3.3MHz$ in wave trains of 25 cycles and 100 Hz rate and placed at a distance of **7 mm** from the interface water-oil. Using the original position of the hydrophone as reference, a scan of 7mm X 7mm with a resolution of 300 µm was done. All these pressure field scans are normalized with respect to the higer value found during its respective measurement. The result is shown below:

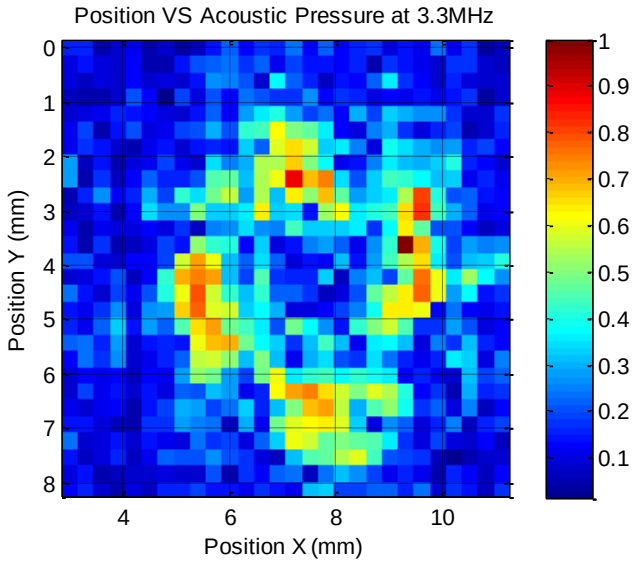

Figure 6. Acoustic Pressure Field as a function of position at 8 mm above the interface.

In this pressure field scan 4 zones of high intensity can be observed, which differs from the expected ring response. To verify this situation, 3 points in the upper part of the ring were selected and a response of pressure field VS frequency was obtained. The three selected points were chosen because of their value of pressure field: a maximal, a minimal and an average pressure field.

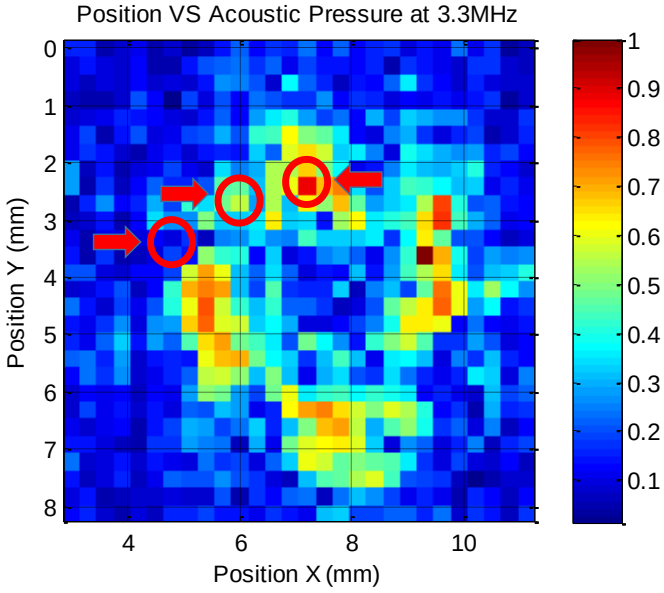

Figure 7. Selected point for the frequency scan.

The results are shown below.

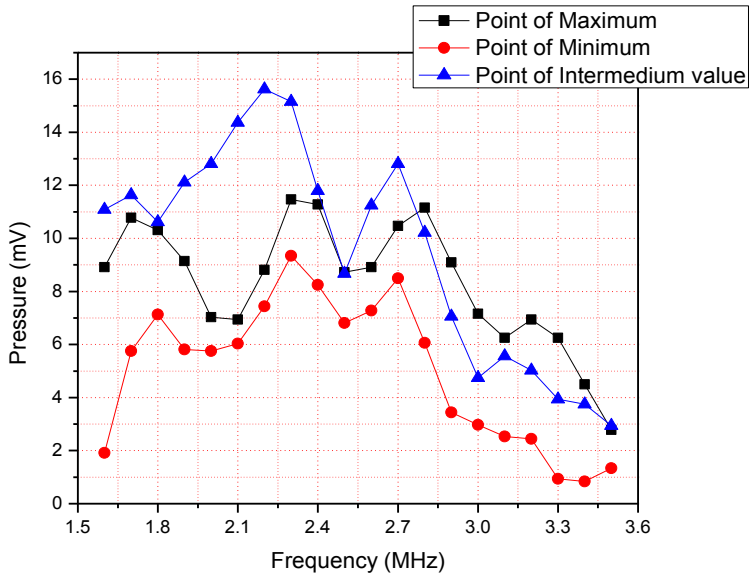

Figure 8. Pressure field response to frequency variation for three points in the annulus.

In this graph, one can see that according to the frequency, the value of the pressure field changes. To verify this, two more measurements were done in different positions.

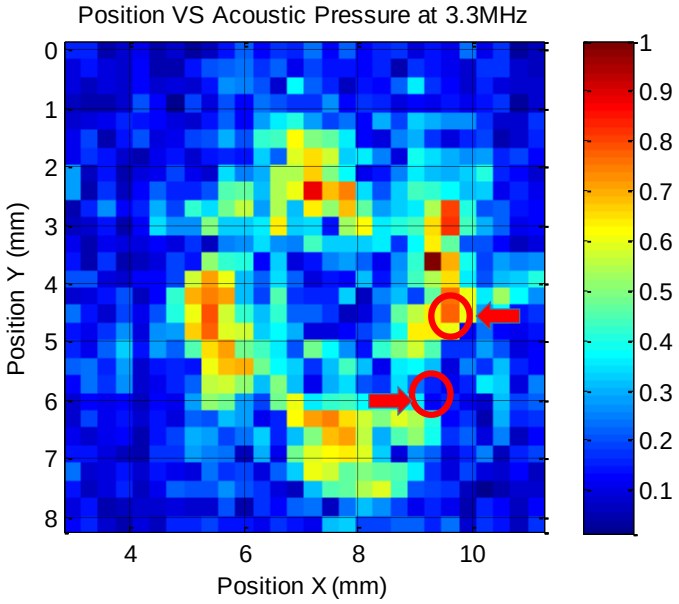

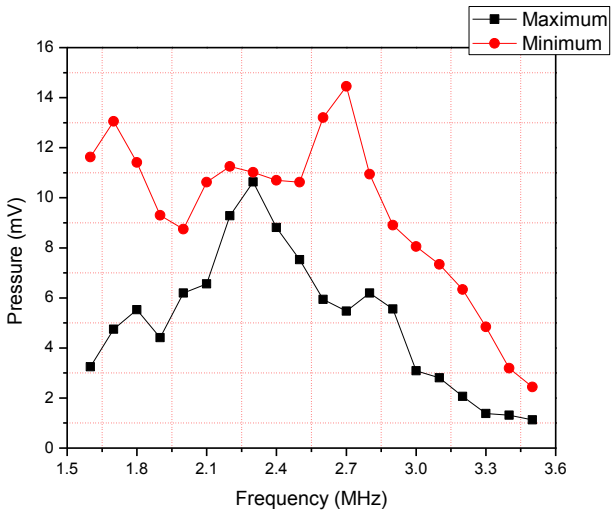

Figure 9. Points selected on the pressure scan and their pressure field response to frequency variation in the annulus.

Comparing both graphs, the pressure field has a smaller difference around a value of frequency equal to 2.5 MHz, so it is expected that a full ring could be get using this frequency value.

A new full pressure field scan versus position was done with a frequency of 2.50 MHz. The resulting mapping is shown below.

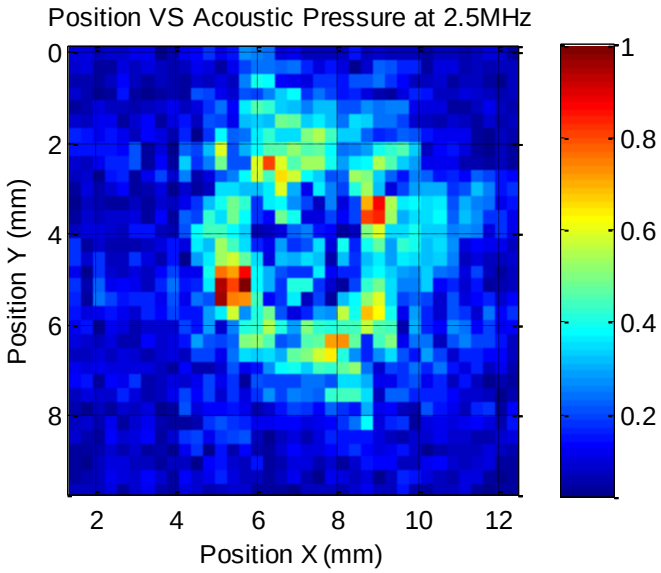

Figure 10. Pressure field VS Position Scan at a frequency of 2.5 MHz, using a resolution of 300 µm.

In this case, it is easier to see the existence of an annulus with more uniform pressure field values, but still one can observe the presence of unwanted dispersion points.

To complete the experiment with a 2.5 MHz frequency, the rotation of the disk was observed at this frequency value. The angular velocity as function of the square of the voltage is shown in figure 11.

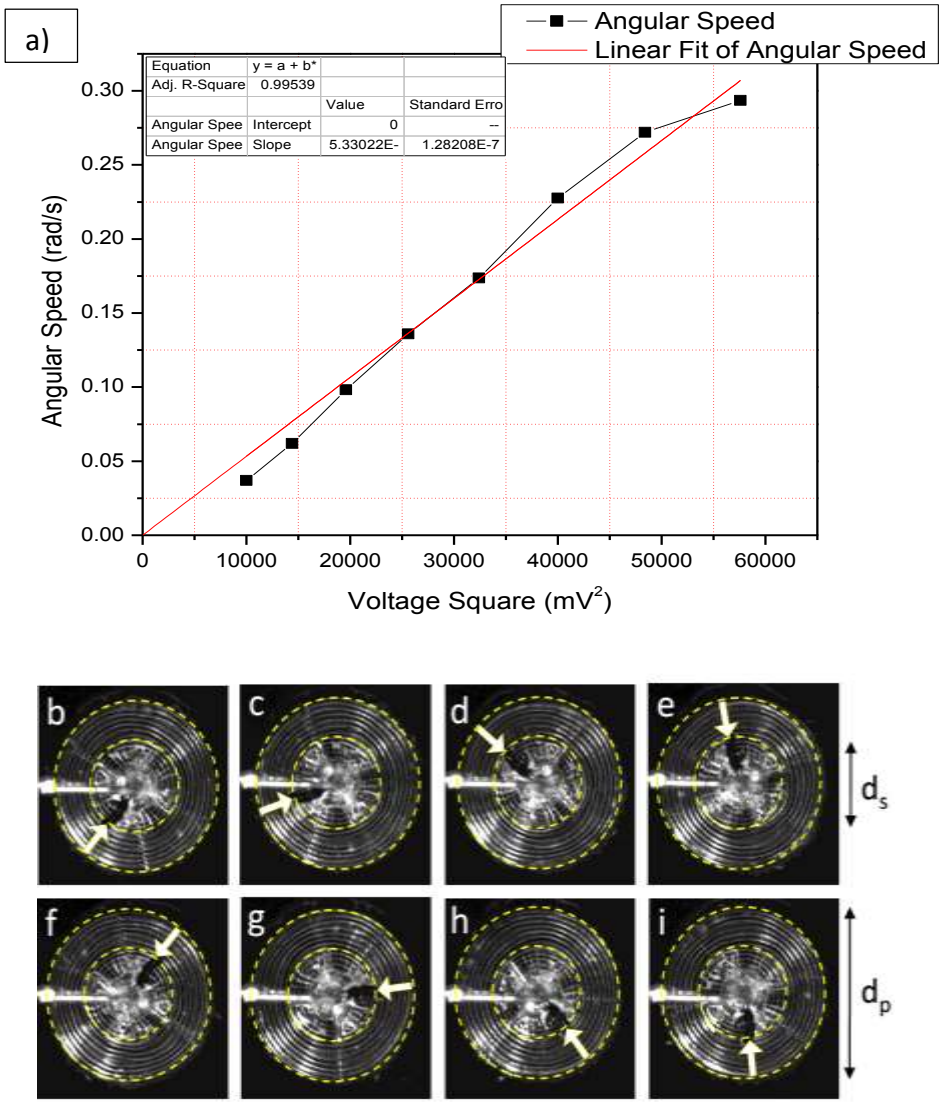

Figure 11. (a) Magnitude of the acoustic SPP rotation angular velocity as a function of U^2 where U is the voltage amplitude applied to the ultrasonic transducer, for $l = 4$. Solid line: linear fit. (b-i) SPP top view snapshots over a full rotation around the z axis, the black radius line on the SPP is an ink mark and the angular displacement between two successive snapshots is roughly $\pi/4$.

In this graph it is possible to see that the solid friction is smaller than at 3.3 MHz and the angular velocity of the system is linear with the square of the input voltage. Also, in

comparison with the results obtained for the 3.3MHz frequency, the sound velocity increased considerably.

A first attempt to explain this behavior was to recalculate the frequency at which the annulus would be optimal by including the factor concerning the angle of incidence of the acoustic waves coming from the transducer with the bottom part of the disk. This is done just by including a simple geometrical consideration in the incident angle.

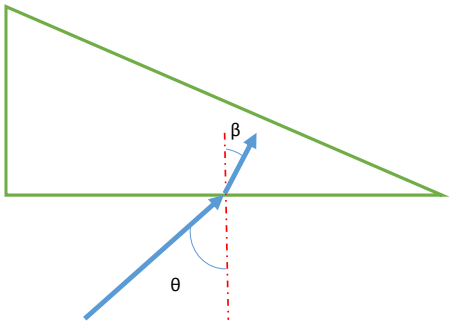

Figure 12. Angle β taken in consideration in the measurements.

Using this angle, the expression to calculate the frequency changes its form to

$$f = \frac{\cos\beta}{\epsilon\left(c_1^{-1} - c_2^{-1}\right)} \tag{4.6}$$

Using this expression and the known parameters of the elements, the frequency obtained is

$$f = 2.861MHz$$

The fact that the value of the optimal frequency changes with the adding of the angle dependence means that any factor can shift this frequency and it should be taken in consideration. As this is an extreme case, it does not explain the value of $f = 2.5MHz$ for which an annulus almost uniform was obtained.

The fact that a spherical transducer is used, suggests that an extreme value of incident angle θ_i is not optimal for the calculation and an effective angle of incidence should be obtained. Furthermore, as the values of sound velocity of salted water and the polylactic acid (PLA) are similar, the angle of incidence θ_i and the angle or refraction β are almost the same.

In order to obtain the value of β_{eff} an average over the surface of the transducer should be done, as shown below.

$$< \beta_{eff} >= \frac{\int \beta ds}{\int ds} = \frac{\int_0^{2\pi} \int_0^r \beta R r d\beta d\varphi}{R^2 \Omega} \quad (4.7)$$

Where Ω is the solid angle for a conic section described by β

$$\Omega = \int_0^{2\pi} \int_0^{\beta} sin\theta d\theta d\varphi = 2\pi \int_0^{\beta} sin\theta d\theta = -2\pi[cos\beta - 1] = 2\pi[1 - cos\beta] \quad (4.8)$$

Looking at a diagram of the system

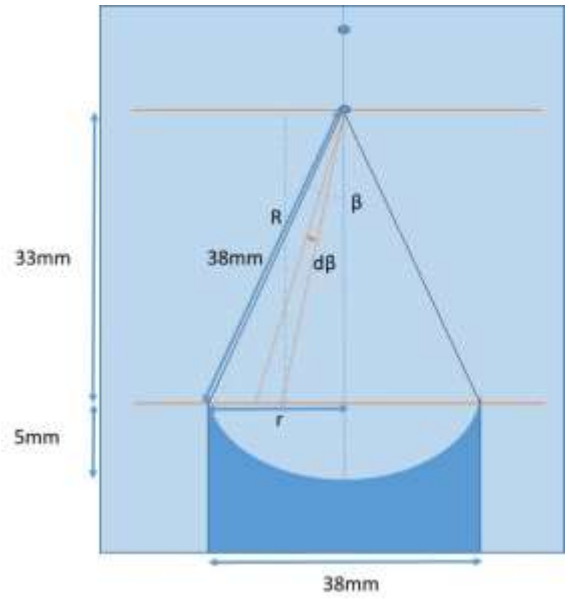

Figure 13. Geometric scheme.

We have that

$$sin\beta = \frac{r}{R} \rightarrow \beta = \arcsin\frac{r}{R}$$

$$d\beta = \frac{1}{\sqrt{1 - \left(\frac{r}{R}\right)^2}} \frac{dr}{R}$$

Then

$$\int_0^{2\pi} \int_0^r \beta R d\beta r d\varphi = 2\pi R \int_0^r \arcsin\left(\frac{r}{R}\right) r \frac{1}{\sqrt{1-\left(\frac{r}{R}\right)^2}} \frac{dr}{R} \quad (4.9)$$

$$= 2\pi R^2 \int_0^r \arcsin\left(\frac{r}{R}\right) \frac{r}{R} \frac{1}{\sqrt{1-\left(\frac{r}{R}\right)^2}} \frac{dr}{R} \quad (4.10)$$

Doing a variable change

$$u = \frac{r}{R}$$

$$du = \frac{dr}{R}$$

$$= 2\pi R^2 \int_0^r \arcsin(u) u \frac{1}{\sqrt{1-u^2}} du \tag{4.11}$$

Integrating by parts, we have

$$= 2\pi R^2 \left[-\sqrt{1-u^2} arcsin(u) + \int du\right] = 2\pi R^2 \left[u - \sqrt{1-u^2} arcsin(u)\right]$$

$$= 2\pi R^2 \left[\frac{r}{R} - \sqrt{1-\left(\frac{r}{R}\right)^2}\, arcsin\left(\frac{r}{R}\right)\right] \tag{4.12}$$

Evaluating in the limit points, r=R/2 and 0, we have

$$= 2\pi R^2 \left[\frac{1}{2} - \sqrt{1-\left(\frac{1}{2}\right)^2}\, arcsin\left(\frac{1}{2}\right) - 0 + \sqrt{1-(0)^2} arcsin(0)\right] \tag{4.13}$$

$$= 2\pi R^2 \left(\frac{1}{2} - \sqrt{\frac{3}{4}} arcsin\left(\frac{1}{2}\right)\right) \tag{4.14}$$

Thus finally one has

$$< \beta_{eff} >= \frac{\int \beta ds}{\int ds} = \frac{\int_0^{2\pi}\int_0^r \beta R d\beta r d\varphi}{R^2\Omega} = \frac{2\pi R^2\left(\frac{1}{2} - \sqrt{\frac{3}{4}} arcsin\left(\frac{1}{2}\right)\right)}{2\pi R^2[1-cos\beta]} \tag{4.15}$$

$$< \beta_{eff} >= \frac{\left(\frac{1}{2} - \frac{\sqrt{3}}{2} arcsin\left(\frac{1}{2}\right)\right)}{[1-\frac{33}{38}]} = .3538 = 20.2712°$$

with

$$cos\beta = \frac{33}{38}$$

Using this value in the relation

$$f_{eff} = \frac{\cos\beta_{eff}}{\epsilon(c_1^{-1} - c_2^{-1})} = \frac{\cos(.3538)}{(1.5mm)(\frac{1}{1460m/s} - \frac{1}{1975m/s})} = 3.5015\ MHz$$

The value in the thickness of the disk has been changed as result of new measurements with a value of 1.5mm.

A new pressure scan was done at 3.5 MHz to observe the behavior of the system, the result is presented below. The position of the hydrophone is located 6.5 mm above the interface.

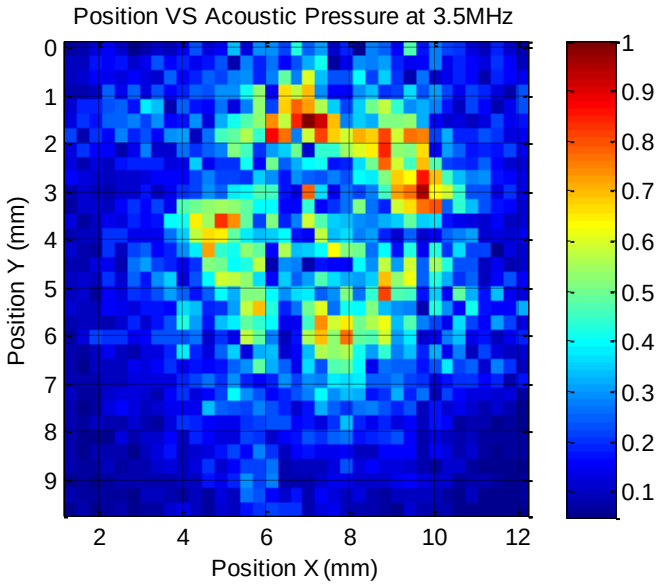

Figure 14. Pressure field VS Position Scan at a frequency of 3.5 MHz, using a resolution of 300 µm.

As can be seen in figure 14, the annulus is not easily distinguishable and the presence of dispersive effects is noticeable. It is necessary to mention that due to the use of a new frequency, the power of the transducer has decreased considerably. As consequence of this reduction of power, the rotation of the disk was not achieved.

As the best results were obtained at 2.5 MHz, it was verified which would be the sound velocity of the PLA in order to have the nice pressure ring, thinking in the ideal case where β is zero.

$$f = \frac{1}{\epsilon\left(c_o^{-1} - c_p^{-1}\right)} \rightarrow \frac{1}{c_p} = \frac{1}{c_o} - \frac{1}{f\epsilon} = \frac{1}{c_p} = \frac{1}{1460 m/s} - \frac{1}{(2.5MHz)(1.5\ mm)} \quad (4.15)$$

$$c_p = 2.39 km/s$$

The response of the system to variations in the sound velocity value for the PLA is really sensible. This could mean that due to the different mechanisms involved in 3D plotting, the sound velocity in the generated disks could be different each time and an absolute value of sound velocity cannot be considered. To see how the sound velocity in the PLA affects the frequency variation a plot is shown below.

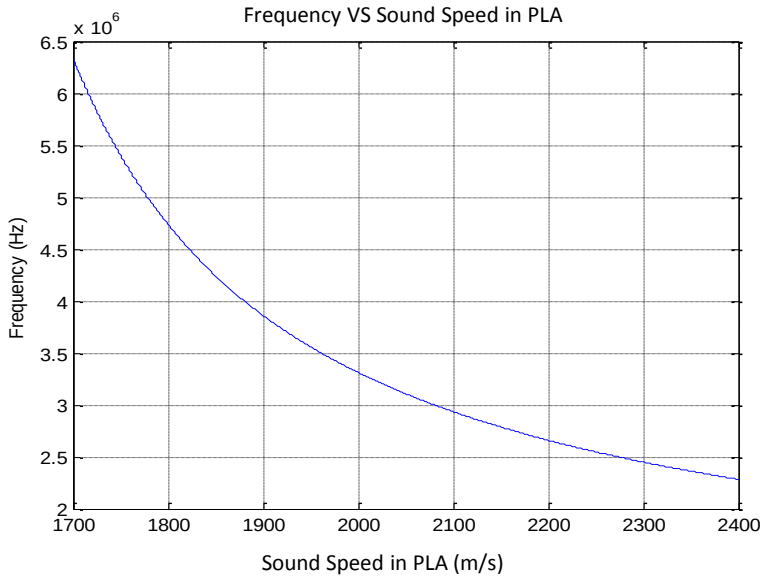

Figure 15. Response of the frequency as function of the sound velocity value of the PLA.

Thus a huge variation of frequency can be expected if there is an uncertainty in the PLA's sound velocity.

As an attempt to obtain a nicer annulus, the spherical transducer was replaced by a planar transducer. The sound field of this kind of transducer is divided into two zones, the near field and the far field. The near field region is the one directly in front of the transducer where the echo amplitude goes through a series of maxima and minima and ends at the last maximum, at distance N from the transducer. The location of the last maximum is known as the near field distance (N) and is the natural focus of the transducer. The far field is the area beyond N where the sound field pressure gradually drops to zero. The near field distance is a function of the transducer frequency, element diameter, and the sound velocity of the test material as

$$N = \frac{D^2 f}{4c} \tag{4.16}$$

For this set up one have

$$N = \frac{D^2 f}{4c} = \frac{(.635cm)^2(2.5MHz)}{4(1783m/s)} = 1.47\ cm$$

This value of N is the current position of the interface and the disk above the planar transducer to have a plane wave. The hydrophone was set 1.4 cm above the interface. As

the diameter of the transducer is around 6 cm, the annulus is expected to have the same diameter. A quick scan was done to obtain the center of the vortex.

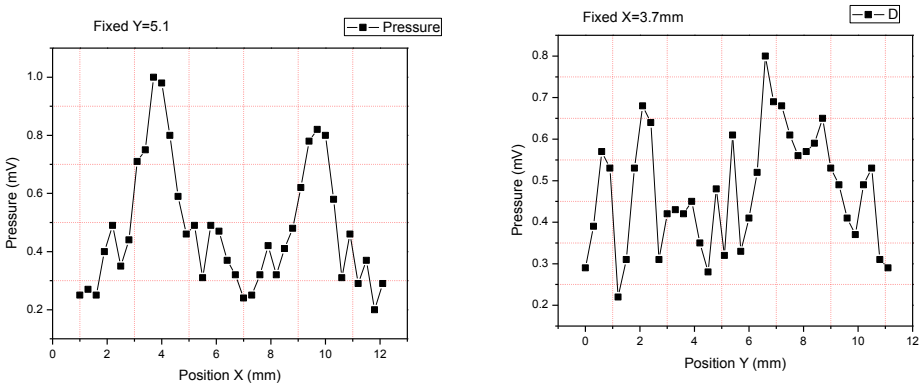

Figure 16. Pressure field VS Position with fixed values of X and Y to find the center of the vortex

Once the center point was found, a quick frequency scan over 6 points was done to verify the existence of an annulus. The results found are shown below.

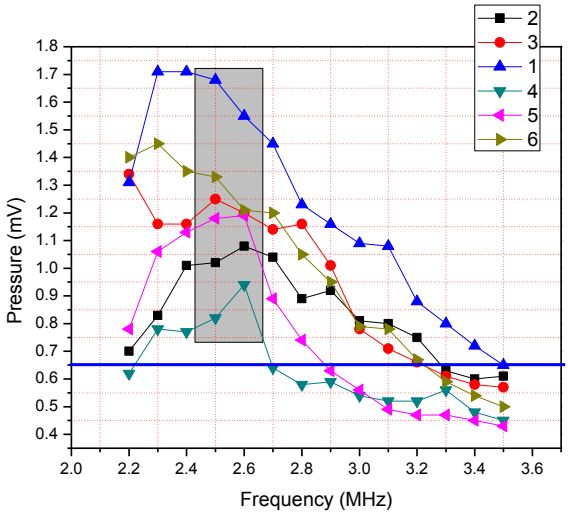

Figure 17. Variation of the pressure field as function of frequency.

It can be seen that not all the points have the same pressure value, meaning that an exact annulus may not be found, but there is a more uniform ring around 2.5 and 2.6 MHz.

The pressure field scan was done with the same parameters as before. The voltage supplied to the transducer was 22.5 Volts with a burst count of 25 cycles at a frequency of 100 Hz. The scan obtained is shown below.

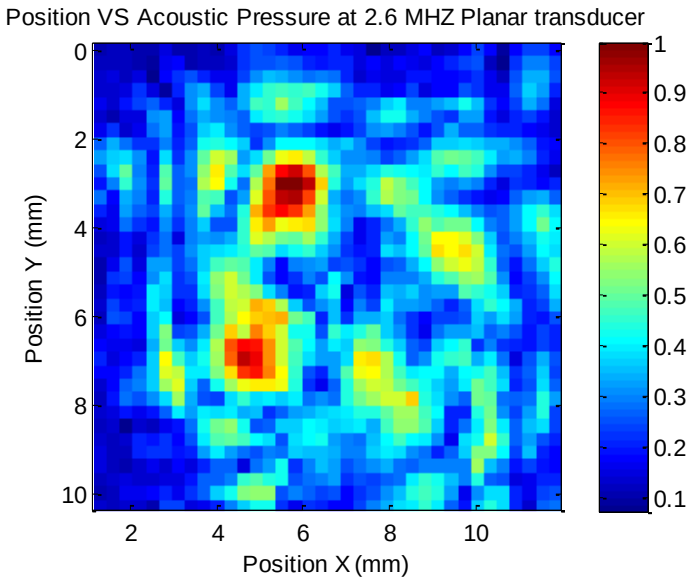

Figure 18. Pressure field VS Position Scan at a frequency of 2.6 MHz, using a resolution of 300 µm.

In this case, diffractive effects are observed due to the shape of the transducer. Also, there are well defined regions of high intensity. This could be caused by the internal structure of the disk, the printing pattern of the 3D printer or the thickness. It seems that the spherical transducer is a better option to achieve a higher interaction between the acoustic wave and the disk.

Finally one can observe from all these results of this particular system that the generation of the disk is not as uniform as wanted. Moreover, small variations of the PLA sound velocity affect considerably the value of the expected effective frequency. Even though good and nice results were found around 2.5 MHz, where solid friction was minimal giving nice exchange of angular momentum and as consequence a nice uniform rotation and a vortex profile for a topological charge of 4 very similar to the expected annulus.

All these results provide good evidence of acoustic orbital angular momentum transfer to matter by chiral scattering. Nevertheless, improvements to the system and the built of the spirals should be done and a deeper analysis of all the variables of the system should be performed in order to fulfill completely the model of angular momentum exchange.

4.2 Acoustic Rotational Streaming

For the second experiment an eight segment transducer was used. The phase delay between each segment of the transducer was given by an electronic circuit previously designed and built in the lab.

Once the system is working, trapping and agglomeration of particles is clearly visible at the focal position of the transducer. Moreover, rotation of the particles is visible for several groups of beads along the propagation axis. For large groups of particles rotation was not visible, but a donut shape patters was observable as shown in figure 19.

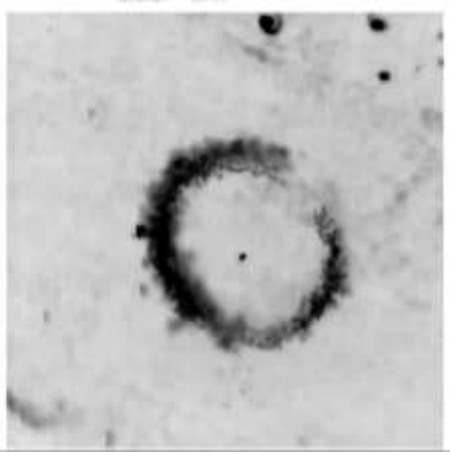

Figure 19. Particles trapped as consequence of the helical wave.

To estimate the size of the observed patterns and trapped particles, a relationship between the amount of pixels per image and a known distance was determined for a specific focal position of the fast camera scope. This relation established that 1 millimeter was equal to 447.6 pixels. This allowed to measure each important visible variable on the recorded images or videos and know the dimensions of it.

The main problem found was that the concentration of the particles is not well-known, this as consequence of the camera saturation. Several trials were made to obtain the optimal visible beads, mainly by varying beads concentration that allowed trapping and nice rotation but taking care to isolate the phenomenon.

It was observed that the system also allows to trap bigger objects, such as bubbles or impurities, and transfer angular momentum.

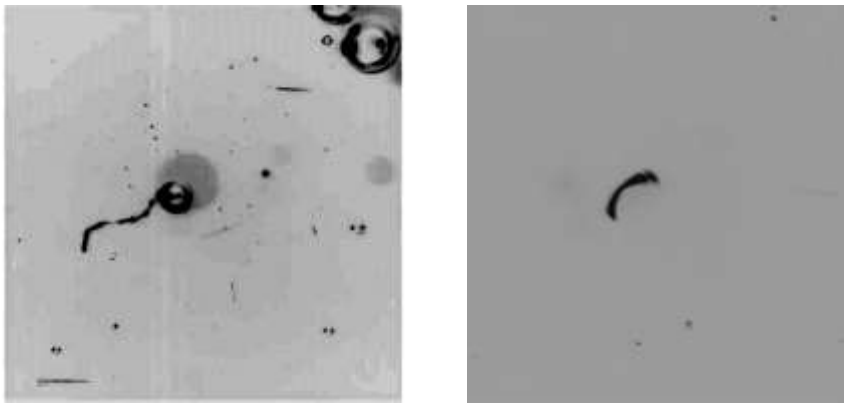

Figure 20. Trapped objects with the helical standing wave

After several trials, the smallest particle density possible was found and used to verify different behavior types of the system. The estimated size of the trapped beads was about 26.84 µm. It is important to mention that the contrast on some images changes due to the fact that the illumination is placed at different angles to observe different particles.

The trajectory of the trapped particle is shown in figure 21. A ring of particles is visible out of focus on the back.

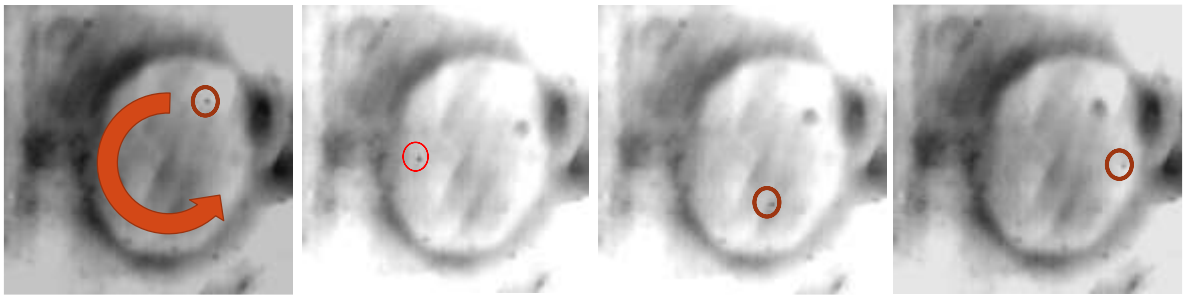

Figure 21. Smaller set of particles trapped and its rotation trajectory.

This set of particles was used to observe the response of the trapping at different voltages, different frequencies and different positions of the opticell along the propagation axis. These responses were visible through the changes in angular velocity of the trapped particle. Results are shown below.

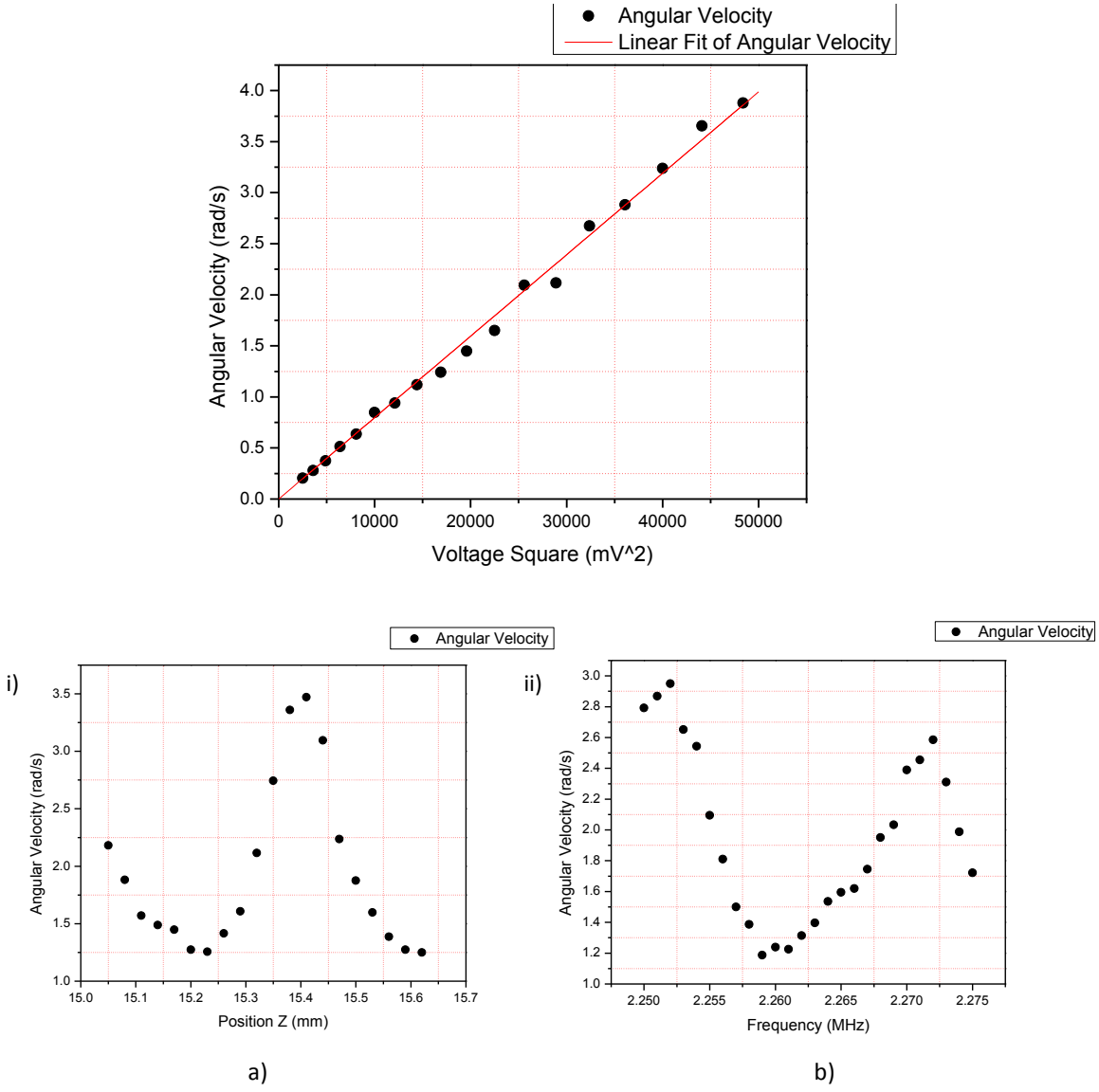

Figure 22. Experimental results of voltage variation, position and frequency for a set of beads of 26 µm diameter.

It is seen from the first graph in figure 22 that the angular velocity is a linear function of the square of the input voltage and no solid friction is noticeable. This result was also seen for other group of particles.

The observed behavior seen in the other graphs, is a consequence of the set-up. The whole system behaves as a Fabry-Pérot cavity [Fig 23], where the mirrors are the transducer on one side and the interface water/air on the other with the opticell placed in the interface.

As the thickness of the opticell's wall are much smaller than the ultrasonic wavelength, it can be assumed that the opticell is "invisible" for this wavelength.

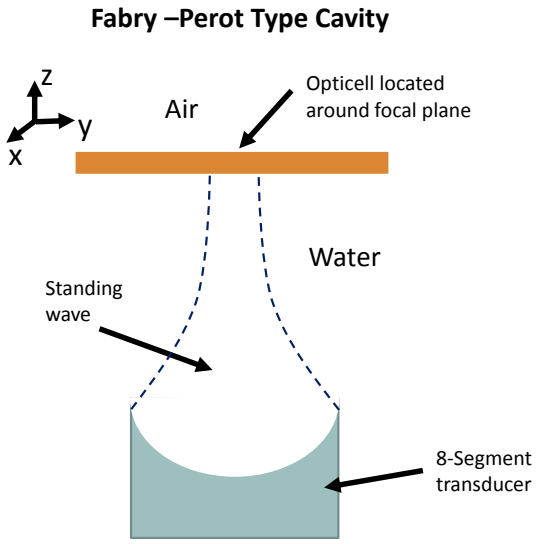

Figure 23. Fabry-Pérot like cavity formed by the transducer and the interface.

Taking this into consideration, changing the frequency or varying the position of the opticell along the propagation axis, changes the dimensions of the cavity, and thus variations of on the number of modes are expected

For a Fabry-Pérot cavity, the number of modes accepted by the cavity is given as

$$n = \frac{2fl}{c} \tag{4.17}$$

Where n is an integer, f is the frequency of the wave, l is the length of the cavity and c the velocity of the wave inside the cavity. For two consecutive modes

$$l = \frac{cn}{2f} = \frac{c(n+1)}{2f'} = \frac{c(n+1)}{2(f+\Delta f)} \tag{4.18}$$

This leads to

$$\frac{f+\Delta f}{f} = \frac{n+1}{n} \rightarrow \frac{\Delta f}{f} = \frac{1}{n} \tag{4.19}$$

If one finds the number of modes inside this specific cavity, one obtains

$$n = \frac{2fl}{c} = \frac{2*2.25*10^6 1/s*38*10^{-3}m}{1500\ m/s} \approx 114$$

And substituting this value in the previous relation, the bandwidth Δf is obtained

$$\Delta f = \frac{f}{n} = \frac{2.25MHz}{114} = 0.0197MHz \approx .02\ MHz \tag{4.20}$$

Comparing this result with figure 22b, it suits nicely.

Doing the same but for the value of l, one obtains

$$\Delta l = \frac{l}{n} = \frac{38\ mm}{114} \approx 0.333mm \tag{4.21}$$

Which is not that different from the observed in figure 22a.

To complete this, it has been demonstrated [3] that a cavity formed by a transducer and an interface behaves as a Fabry- Pérot cavity with a transmittance coefficient given as

$$P_i = \left|1 - RR'exp\left(i\frac{4\pi(L+h)}{\lambda}\right)\right|^{-1} P \tag{4.22}$$

Where $R$and $R'$are the reflectance coefficients of the transducer and the interface air-water with values $R = -0.455,\ \ R' = -1,\ \ L = 38mm,\ \lambda \approx 660\ \mu m$ and h the position above the transducer..

Plotting this equation as function of position along the propagation axis (h variable) and different frequencies and comparing with obtained data, one obtains

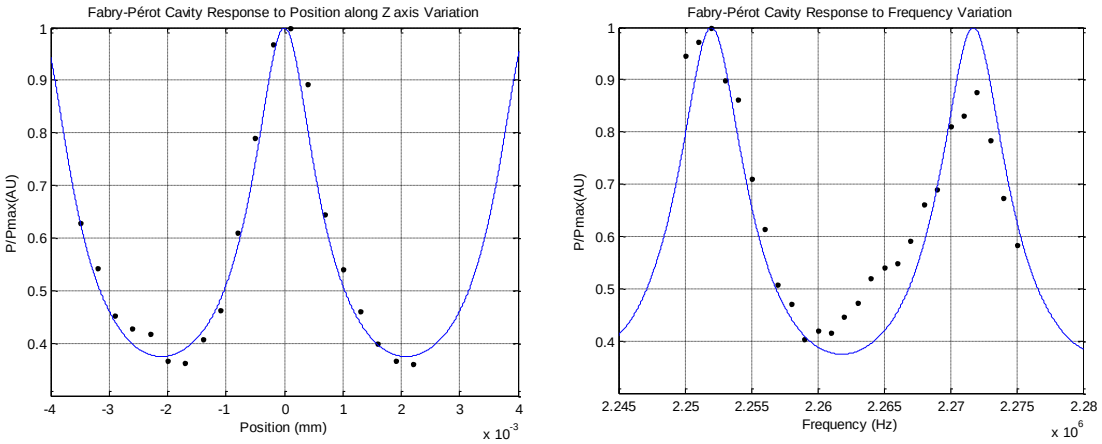

Figure 24. Data fitting to model of the Fabry Pérot cavity for a value of R=0.455

The obtained results fit nicely with the known theory.

As it was told before, a stationary wave is formed inside the cavity. This standing wave along the propagation axis has nodes and antinodes where the particles should be trapped due to the gradients of pressure.

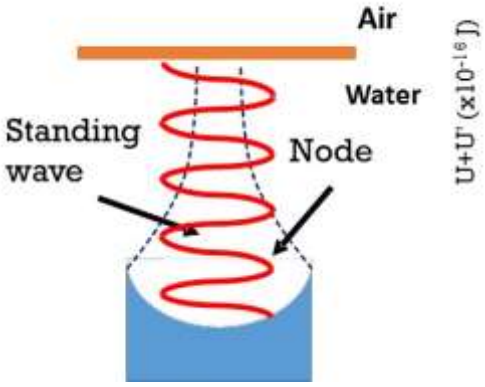

Figure 25. Standing wave inside the cavity and the allowed modes inside it.

With the calculations done before, one expect to have at least 6 modes inside the opticell, this is 6 groups of particles trapped at different positions along the opticell. Nevertheless, as PMMA beads cannot be nicely manipulated or even separated fully; this means that observing 6 “levels” of particles is ideal. Many attempts were done to trap and rotate particles at these different nodes. To measure the distance between these levels, the camera was displaced using a micrometer plate, changing its focal plane of position and focusing on the images at different levels as shown in figure 26.

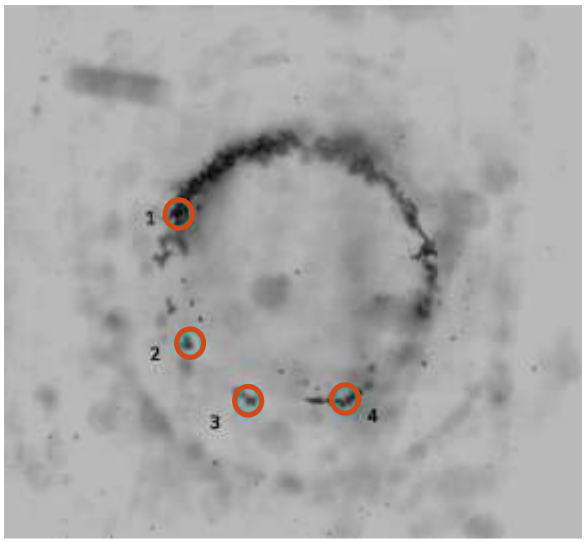

Figure 26. Group of beads used to measure the separation between levels along the Z axis.

The distances measured between these levels were

Level	Position Relative (mm)	Difference between previous (mm)
Wall of Opticell	7.79	
1	7.42	0.37
2	7.05	0.37
3	6.78	0.27
4	6.49	0.29

From these obtained values, one can observe that these levels are located near a value of $\frac{\lambda}{2} \approx .33\, mm$ as expected. The error associated to this measurement comes from the resolution criteria, as in some cases a group of particles seemed to have certain thickness. This levitation of particles in a liquid can be explained as follows.

In the following, index 0 refers to the liquid, 1 to the particle. At the water-air interface, due to the large impedance mismatch, a pressure release boundary condition is assumed for the reaction of the up-propagating wave. Assuming a plane, standing wave and pressure release condition at z = 0 (z is the depth below the air-water interface), the complex pressure can be written as:

$$p = Asin(k_0 z)\exp(-i\omega t) \tag{4.23}$$

(Note the zero of pressure at the interface (z = 0)).

The acoustic levitation potential U is [1]:

$$U = \frac{2\pi R^3}{\rho_0 c_0^2}\frac{A^2}{2}\left(\frac{f_1}{3}sin^2(k_0 z) - \frac{f_2}{2}cos^2(k_0 z)\right) \tag{4.24}$$

Where $f_1 = 1 - \frac{1}{\lambda\sigma^2}\left(\lambda = \frac{\rho_1}{\rho_0} \quad and \quad \sigma = \frac{c_1}{c_0}\right)$ and $f_2 = \frac{2(\lambda-1)}{2\lambda+2}$.

The potential associated with the weight and buoyancy is

$$U' = -\frac{4}{3}\pi R^3(\rho_1 - \rho_2)gz \tag{4.25}$$

(sign – is because z is the depth below the surface, not the altitude). The total potential encountered by the particle is $U + U'$. This potential behaves as shown in figure 27.

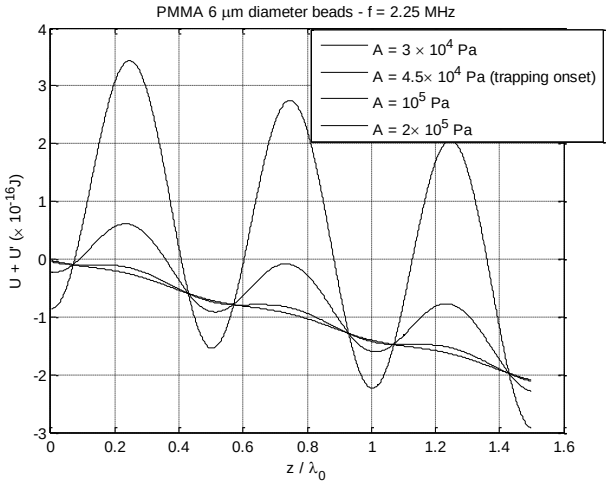

Figure 27. Potential over a particle immerse on a pressure field at different amplitudes.

Even when this calculation is a simple model, the behavior observed in the potential fits the observed results. A minimum in potential value is found every $\frac{\lambda}{2}$, this means that the particles get trapped along the z axis every time a distance multiple of $\frac{\lambda}{2}$ is reached. This is in total agreement with the distances found in the experiment. The higher the amplitude pressure, the greater the potential and stronger the force over the trapped particles.

With the images and videos captured, the trajectory and diameter of the donut drawn by the particles were obtained. This was done using an image processing software called FIJI.

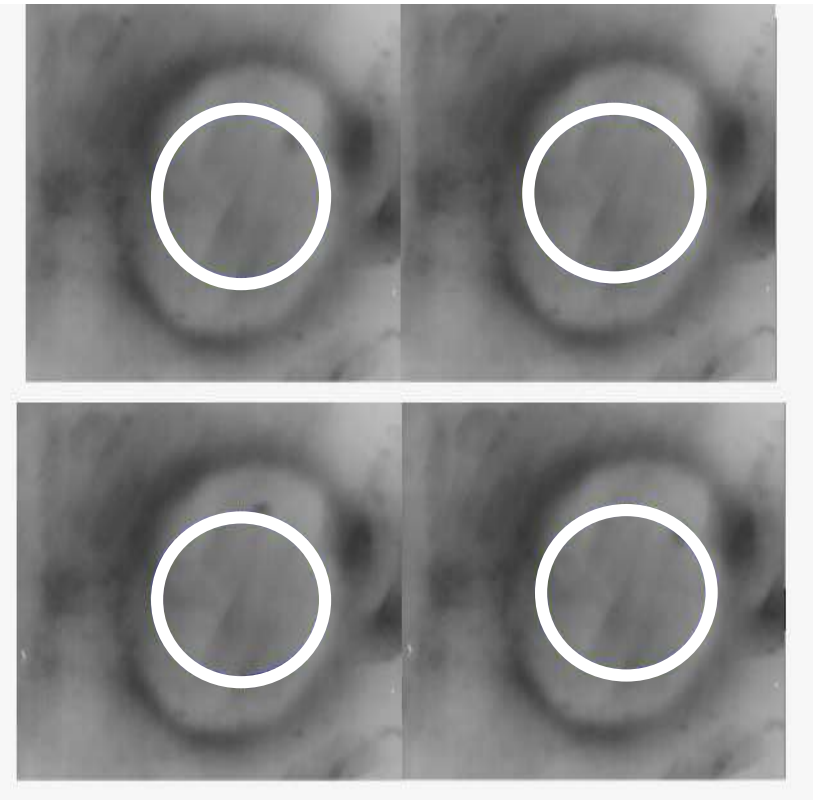

Figure 28. Observed trajectories for some positions along the Z axis.

As all the trajectories were compared and all the diameters measured,iIt was noticed that these changed along different positions and frequencies. It was visible that at different points the ellipticity of the trajectory and the diameter changed its size. This was expected since we are affecting the cavity and thus the parameters involved.

The problem in the measurement of the diameter and the trajectories is that as the system is not able to be perfectly aligned, when the opticell is displaced a small tilt appears. This tilt may be responsible for the effect of ellipticity in the different trajectories. Even when it is not accurate, a measurement of the diameter as function of the position was done.

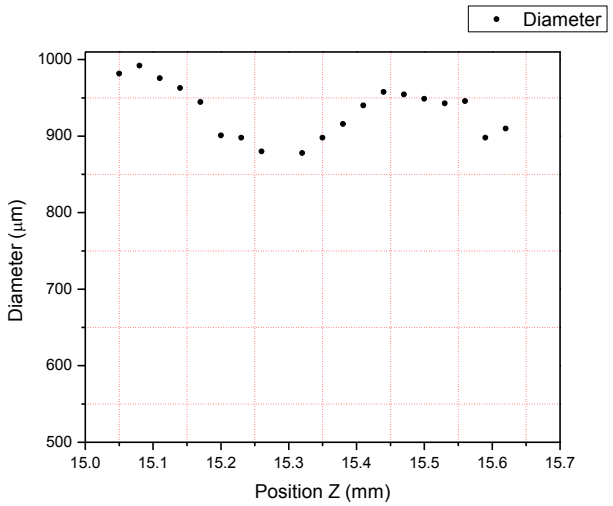

Figure 29. Diameter of the trajectory as a function of Position along the propagation axis

The important thing about this graph is that the diameter's size is always below 1 mm and above 800 μm, and recalling figure 17 in the previous chapter, this is an approximate interval for the diameter of the donut profile found. This would mean that rotation is due to the presence of the helical wave.

To sustain this point and prove that is not just radiation pressure from the field, the phase delay system was removed and particles were tried to be manipulated with the focused beam. The observed pattern is shown below compared with a donut shape one.

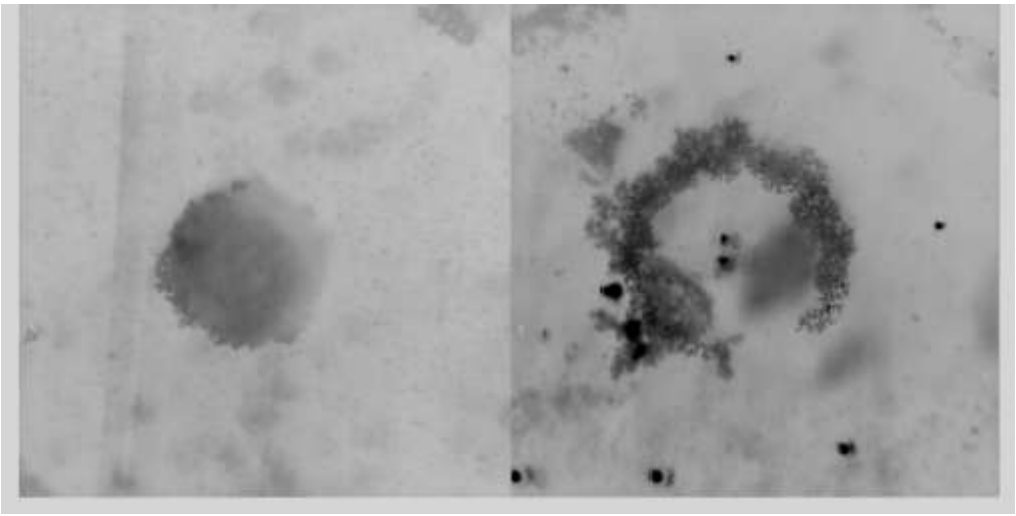

Figure 30. Patterns observed. On the left the transducer without the phase delay and on the right with the phase delay.

It was clearly visible that the beam with no phase delay did not generate a donut beam neither a stream that rotates the beads. The beads just agglomerate in the focus point and gather there. On a second plane at the back of this bulk of particles, a nice ring is visible which corresponds to the first zero of the Bessel function profile. The opticell was manipulated to induce a tilt to see if it was possible to observe rotation. This was visible but in a much smaller magnitude as the beam with helical phase. Nevertheless, if the tilt was eliminated, this small rotation was also eliminated. To verify that the observed rotation with the helical beam was not induced by the tilt, the experiment was repeated varying this tilt in different directions. It did not matter how much tilt was introduced, the particle still rotated but had its trajectory deformed. This could explain the change in ellipticity in the previous measurements.

To confirm that the effects observed were due to the presence of acoustic rotational streaming and not radiation pressure or other effects, several recordings were done beginning with the system in a stationary state when the transducer was turned off until the moment when the transducer is switched on and the system reaches stability. It was clearly visible that when the system was switched on, a stream corresponding to the exchange of angular momentum between the wave and the liquid was present, this is confirmed because the flux is over all the particles and not only local, which would only affect certain particles at certain locations as seen in figure 31.

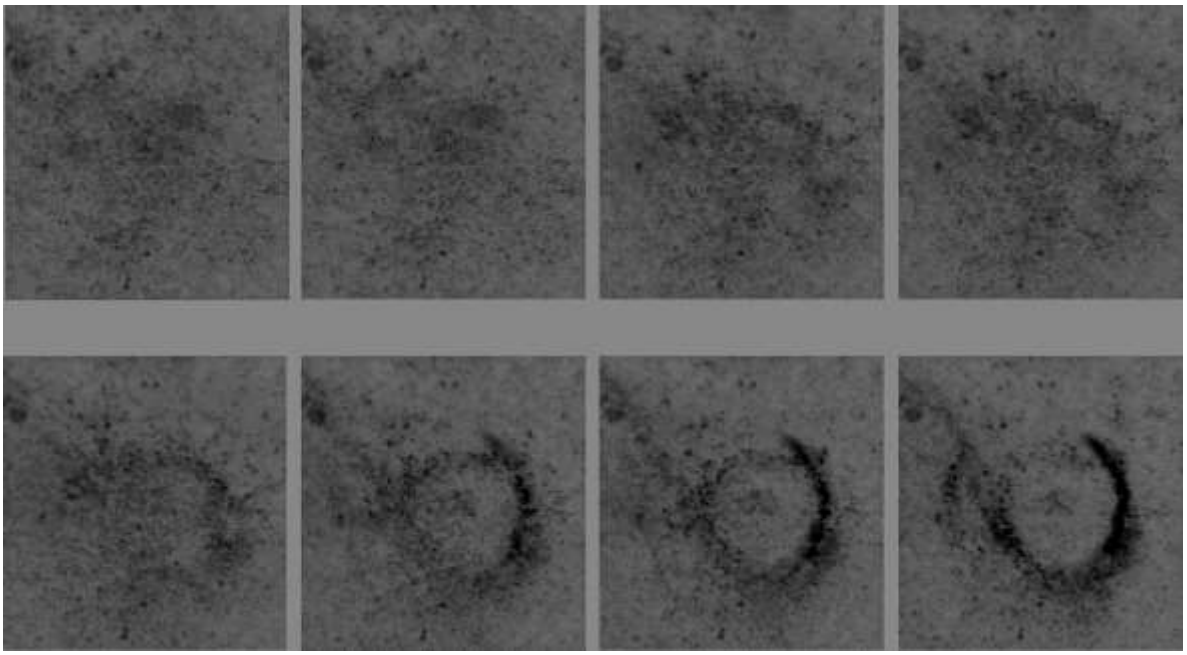

Figure 31. Evolution of the beads pattern from its stationary state to the point of stability when the streaming is present. The stream goes in counter clockwise direction in agreement with the direction of the acoustic vortex.

One important question in this experiment was if it is possible to assure that the beads are good tracers of the generated stream inside the opticell. To evaluate this, the computation of the orthoradial force experienced by an individual particle was done to evaluate if the particles used to image the fluid rotation follow the liquid or not. It is known that particle clusters scatter sound more than all the individual particles but still this computation gives a nice approximation of the experienced situation.

Considering index 0 as the liquid one, 1 to the particle: $\rho_0 = 1000\ kg \cdot m^{-3}$, $\rho_1 = 1188\ kg \cdot m^{-3}$, $c_0 = 1490\ m \cdot s^{-1}$, $c_1 = 2690\ m \cdot s^{-1}$. The particle radius is $a = 3\ \mu m$ and $\lambda = 660\ \mu m$. The fluid has dynamic viscosity $\upsilon = 10^{-6}\ m^2 \cdot s^{-1}$.

In the $a \ll \lambda$ limit, and taking into account the viscous effects, the radiation force experienced by a rigid, spherical particle with radius a irradiated by a progressive wave is [4]:

$$\mathbf{F}_{rad} = f\left(\tilde{\rho}, \tilde{\delta}\right)\pi a^3 \frac{\omega}{\rho_0 c_0^3}\langle p^2\rangle \mathbf{n} \tag{4.26}$$

Where ω is the acoustic pulsation, p is the pressure fluctuation amplitude, $\mathbf{n} = \frac{\mathbf{k}}{k}$,

$$f\left(\tilde{\rho}, \tilde{\delta}\right) = \frac{6(1-\tilde{\rho})^2\left(1+\tilde{\delta}\right)\tilde{\delta}}{(1-2\tilde{\rho})^2+9(1+2\tilde{\rho})\tilde{\delta}+\frac{81}{2}\left(\tilde{\delta}^2+\tilde{\delta}^3+\frac{1}{2}\tilde{\delta}^4\right)} \approx 0.002 \tag{4.27}$$

With $\tilde{\delta} = \frac{\delta}{a}$, $\delta = \sqrt{\frac{2\nu}{\omega}}$ the viscous boundary layer thickness, and $\tilde{\rho} = \frac{\rho_1}{\rho_0}$. Since the particles used in the experiment are not rigid compared to water, this expression over- estimates de radiation force.

Although the vertical and radial components of the acoustic field experienced by the trapped particles are stationary, the orthoradial components of the Poynting vectors associated to the forward (upward) and the backward (downward) vortex beams are parallel, not antiparallel, so the orthoradial component of the acoustic field is progressive-like. This is why the formulas valid for a progressive wave are used for the evaluation of the orthoradial radiation force. However, the question of the actual radiation force exerted by a r- and z- standing, θ- progressive wave is open.

The angle between the beam axis and the Poynting vector is $\theta = \frac{l}{kr}$, where l is the vortex topological charge and r the distance to the axis. So the orthoradial force intensity experiences by the particle is $\mathbf{F}_{rad} sin\theta$. The particles are trapped along the pressure maximum circle defined by $kr = 5$ [2] and $l = 1$.

What is the drift velocity due to radiation force? Since the Reynolds number associated to the flow around the particles is $Re \ll 1$, the particle with velocity V relatively to the surrounding fluid experiences a Stokes-like drag force $6\pi\eta aV$.

Hence, $= \frac{F_{rad}\sin(1/5)}{6\pi\eta a}$. V must be compared to the fluid rotation velocity predicted by [2]

$$u = \frac{3\alpha\omega_0}{\omega\rho_0 c_0 \eta}\langle p^2\rangle \frac{1-exp(-2x^2)}{16x} \tag{4.28}$$

Where $x = \frac{r}{\omega_0}$, $\omega_0 = 1.025\lambda$, α is the attenuation coefficient, $kr = 5$ corresponds to $x = \frac{5}{2\pi * 1.025} \approx 0.78$, for which $\frac{1-exp(-2x^2)}{16x} \approx 0.56$. Finally

$$\frac{V}{u} \approx 2 * 10^{-4} \frac{(ka)^2 \sin(1/5)}{\alpha\omega_0} \tag{4.29}$$

With $ka \approx 2 - 9 * 10^{-2}$ and with $\alpha = 0.041 m^{-1}$, one finds $\frac{V}{u} = 0.0012 \ll 1$. So the particles are tracers for the rotation flow.

Finally, a full scan of the transducer profile was done to verify its symmetry and that the pressure profile was uniform along the donut. The resolution used was 100 µm.

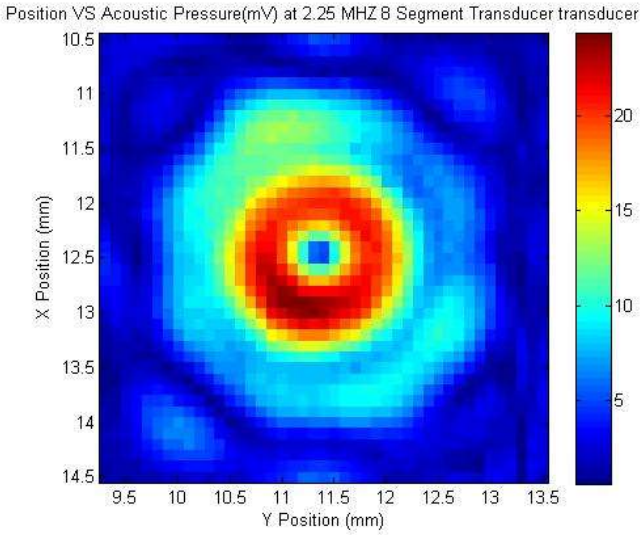

Figure 32. Donut shape profile of the transducer.

This profile lets us see that the traced path drawn by the particles is in total agreement with the dimensions of the vortex with a diameter of 1 mm along the donut. An important spot of higher pressure is found. In the analysis of the videos, in this region of the field the particles accelerated meanwhile in other regions it was uniform.

After all these results, the existence of acoustic rotational streaming is evident. There is a consistence in the basic theory used and the experimental observed results.

4.3 References

[1] M. F. Hamilton, D. T. Blackstock, Nonlinear Acoustics, Academic Press, (1998).

[2] A. Anhäuser. Rotation, twist and flow induced by an intense acoustic vortex beam. Université Bordeaux 1. (2011).

[3] B. Issenmann, R. Wunenburger, S. Manneville, J. P.Delville, Biestability of a compliant cavity induced by acoustic radiation pressure. Phys. Rev. Lett. 97, 074502 (2006).

[4] M. Settnes, H. Bruus. Forces acting on a small particle in an acoustical field in a viscous fluid. Phys. Rev. E85, 016327 (2012).

Chapter 5

Conclusions

In the present work results on the study of acoustic vortices have been shown, more specifically the transfer of acoustical angular momentum between an ultrasonic wave and matter and the effect called acoustic rotational streaming due to the exchange of angular momentum between an ultrasonic wave and a fluid.

Regarding the first topic, rotation induced by an intense acoustic vortex beam is observed. For this case, the exchange of angular momentum by chiral scattering was searched. We report on orbital angular momentum exchange between sound and matter mediated by a non-dissipative chiral scattering process.

The generation and manipulation of the spiral with sound was observed. The exchange of angular momentum was achieved successfully, as theory predicted. It was seen that high powers are required to rotate the disk at a uniform velocity.

Moreover chiral refraction is shown to impart a nonzero orbital angular momentum to the scattered field and to rotate the object. For the optimal working frequency, this rotation of the disk present none solid friction with the media.

Experimentation and analysis of the system indicate that the exchange of momentum is easily affected by the velocity value of the PLA. Small variations on this value change the effective working frequency and reduce the effect. This variations of the velocity are due to the construction of the spiral plate, it could be the presence of small air bubbles or irregularities in the printing of the structure.

As a consequence of these variations of velocity in PLA, the expected profile for a vortex of topological charge $l = 4$ is not fully achieved instead a non-uniform annulus is observed. If the velocity in the disk was uniform along the whole disk, this annulus should be equal to the predicted by theory.

This results constitutes a proof-of-concept of a novel kind of acoustic angular manipulation of matter.

Concerning the second topic, the exchange of acoustic angular momentum between a helicoidal wave and a fluid was studied, specifically the effect known as acoustic rotational streaming. The first direct experimental demonstration of this effect was achieved and observed.

To achieve this, the generation and characterization of an acoustic vortex with topological charge $l = 1$ was done using an eight segment transducer.

It was observed that the system behaved as a Fabry –Pérot cavity for an acoustic wave. This cavity was analyzed theoretically and results were in total agreement with the experiment.

A simple mathematical model for the beads inside the pressure field was given and data agreed with it. To fully comprehend this phenomenon, further investigation must be done involving the different parameters involved in the experiment.

As it is a small phenomenon, acoustic rotational streaming is not easily observed and several improvements should be done to the system and the model to completely understand it.

As the first direct experimental observation of this phenomenon, this represents a big contribution to the field of non-linear acoustics and gives a new tool in acoustics research.

Further Work

For the experiment concerning the transfer of angular momentum from an acoustic wave to matter requires a deeper characterization of the PLA phase disks. Each plate must be characterized individually after its generation in the 3D printer.

In order to reduce the measuring time in each pressure profile measured, an automatization of the system should be done, as well as an improvement in the measuring method.

For the second experiment, a deeper study of the variables involved in the acoustic rotational streaming phenomenon should be done. More parameters should be taken into consideration to explain unanswered questions observed during the experiment realized.

Different sizes and types of beads should be used as tracers to observe the behavior of the system and possible differences in responses.

Finally a more effective experiment should be design to isolate a much smaller number of beads to observe with a higher quality this effect.